Research

New Phytologist

Arabidopsis Topless-related 1 mitigates physiological damage and growth penalties of induced immunity

Thomas Griebel[1,2]*, Dmitry Lapin[1,3]*, Federica Locci[1], Barbara Kracher[1], Jaqueline Bautor[1], Lorenzo Concia[4], Moussa Benhamed[4] and Jane E. Parker[1,5]

[1]Department of Plant–Microbe Interactions, Max-Planck Institute for Plant Breeding Research, 50829 Cologne, Germany; [2]Dahlem Centre of Plant Sciences, Plant Physiology, Freie Universität Berlin, 14195 Berlin, Germany; [3]Translational Plant Biology, Department of Biology, Faculty of Science, Utrecht University, 3584 CH Utrecht, the Netherlands; [4]Institute of Plant Sciences Paris-Saclay (IPS2), CNRS, INRA, University Paris-Sud, University of Evry, University Paris-Diderot, Sorbonne Paris-Cite, University of Paris-Saclay, Batiment 91405 Orsay, France; [5]Cluster of Excellence on Plant Sciences (CEPLAS), 40225 Düsseldorf, Germany

Authors for correspondence:
Jane E. Parker
Email: parker@mpipz.mpg.de

Dmitry Lapin
Email: d.lapin@uu.nl

Thomas Griebel
Email: thomas.griebel@fu-berlin.de

Received: *12 November 2022*
Accepted: *9 May 2023*

New Phytologist (2023) **239:** 1404–1419
doi: 10.1111/nph.19054

Key words: ChIP-Seq, corepressor, immunity, resilience, Topless-related 1.

Summary

- Transcriptional corepressors of the Topless (TPL) family regulate plant hormone and immunity signaling. The lack of a genome-wide profile of their chromatin associations limits understanding of the TPL family roles in transcriptional regulation.
- Chromatin immunoprecipitation with sequencing (ChIP-Seq) was performed on *Arabidopsis thaliana* lines expressing GFP-tagged Topless-related 1 (TPR1-GFP) with and without constitutive immunity via *Enhanced Disease Susceptibility 1* (*EDS1*). RNA-Seq profiling of the TPR1-GFP lines and pathogen-infected *tpl/tpr* mutants, combined with measuring immunity, growth, and physiological parameters was employed to investigate TPL/TPR roles in immunity and defense homeostasis.
- TPR1 was enriched at promoter regions of *c*. 1400 genes and *c*. 10% of the detected binding required *EDS1* immunity signaling. In a *tpr1 tpl tpr4* (*t3*) mutant, resistance to bacteria was slightly compromised, and defense-related transcriptional reprogramming was weakly reduced or enhanced, respectively, at early (< 1 h) and late 24 h stages of bacterial infection. The *t3* plants challenged with bacteria or pathogen-associated molecular pattern nlp24 displayed photosystem II dysfunctions. Also, *t3* plants were hypersensitive to phytocytokine pep1 at the level of root growth inhibition. Transgenic expression of *TPR1* rescued these *t3* physiological defects.
- We propose that TPR1 and TPL family proteins function in *Arabidopsis* to reduce detrimental effects associated with activated transcriptional immunity.

Introduction

Plant disease resistance to pathogenic microbes is mediated by cell surface and intracellular immune receptors (Cui *et al.*, 2015; Jones *et al.*, 2016; Albert *et al.*, 2020). Extracellular leucine-rich repeat (LRR) domain receptors recognize pathogen-associated molecular patterns (PAMPs) or host-secreted phytocytokine peptides to confer pattern-triggered immunity (PTI; Albert *et al.*, 2020). Intracellular nucleotide-binding domain/LRR (NLR) immune receptors intercept pathogen virulence factors (called effectors) after their delivery to host cells to produce effector-triggered immunity (ETI). These two receptor systems cooperate to provide robust resistance, often associated with localized host cell death (Ngou *et al.*, 2021; Yuan *et al.*, 2021).

All tested NLR members with N-terminal Toll and interleukin-1 receptor domains (referred to as TIR-NLRs or TNLs) and some cell membrane-resident receptor-like proteins (RLPs) signal via the nucleo-cytoplasmic immunity regulator Enhanced Disease Susceptibility 1 (EDS1; Fradin *et al.*, 2011; Lapin *et al.*, 2020; Dongus & Parker, 2021; Pruitt *et al.*, 2021). EDS1 forms exclusive, functional heterodimers with its sequence-related partners Phytoalexin Deficient 4 (PAD4) and Senescence-associated Gene 101 (SAG101; Wagner *et al.*, 2013; Sun *et al.*, 2021). The EDS1 heterodimers promote timely transcriptional upregulation of defenses in *Arabidopsis thaliana* (hereafter *Arabidopsis*), which is necessary for NLR-mediated bacterial resistance (Cui *et al.*, 2018; Mine *et al.*, 2018; Bhandari *et al.*, 2019).

In *Arabidopsis*, WRKY family transcription factors (TFs; Tsuda & Somssich, 2015; Birkenbihl *et al.*, 2017; Zavaliev *et al.*, 2020), Systemic Acquired Resistance Deficient 1 (SARD1) and its homolog Calmodulin-Binding Protein 60-like g (CBP60g; Sun *et al.*, 2015; Ding *et al.*, 2020) have prominent roles in early transcriptional mobilization of defenses. As part of a network with WRKY TFs, CBP60g, and SARD1 help to boost the *Isochorismate Synthase 1* (*ICS1*) expression, biosynthesis and signaling of the defense hormone salicylic acid (SA) in response to pathogen attack (Zhang *et al.*, 2010; Zhou *et al.*, 2018). These TFs are further transcriptionally induced in response to salicylic

*These authors contributed equally to this work.

acid (SA; Hickman *et al.*, 2019). A myelocytomatosis (MYC) TF, MYC2, controls signaling by the defense hormone jasmonic acid (JA; Lorenzo *et al.*, 2004; Zander *et al.*, 2020). The SA- and JA-dependent signaling branches can antagonize each other, and bacteria employ effector molecules such as coronatine, a structural mimic of JA, to manipulate the hormonal crosstalk (Zheng *et al.*, 2012; Yang *et al.*, 2017). Coronatine-mediated hijacking of JA/MYC2 pathway to dampen SA-dependent defense is blocked in ETI mediated by the TNL pair Resistant to *Ralstonia solanacearum* 1 (RRS1) and Resistant to *Pseudomonas syringae* 4 (RPS4) in *Arabidopsis* (Sohn *et al.*, 2014; Cui *et al.*, 2018; Bhandari *et al.*, 2019). In $TNL^{RRS1\text{-}RPS4}$ ETI, EDS1 enables a timely boost of SA-regulated transcription and suppression of the JA/MYC2-dependent gene expression to restrict bacterial growth (Cui *et al.*, 2018; Bhandari *et al.*, 2019).

Activated defenses can have detrimental effects on plant physiology and growth if they are prolonged or constitutive (Todesco *et al.*, 2010; Ariga *et al.*, 2017; Caarls *et al.*, 2017; van Butselaar & Van den Ackerveken, 2020; Bruessow *et al.*, 2021). DNA methylation and polycomb-dependent H3K27me3 marks, which deplete during plant defense reactions (Dowen *et al.*, 2012; Yu *et al.*, 2013; Dvořák Tomaštíková *et al.*, 2021), small RNAs, and ubiquitin ligase-mediated protein degradation help to limit *NLR* expression and growth penalties in uninfected plants (Deng *et al.*, 2017; Zervudacki *et al.*, 2018; Copeland & Li, 2019; Huang *et al.*, 2021; Qiao *et al.*, 2021). However, the processes of transcriptional restriction of potentially dangerous induced immunity after pathogen detection are still poorly understood.

Transcriptional corepressors form a layer of gene expression control in eukaryotes. Plant Topless (TPL) and Topless-related (TPR) corepressors resemble Groucho/Tup1 transcriptional corepressors and carry a WD40 repeat C-terminal region and several N-terminal domains (Martin-Arevalillo *et al.*, 2017; Plant *et al.*, 2021). Via the N-terminal domains, TPL/TPRs interact with ethylene response factor (ERF) – amphiphilic repression (EAR) motifs present in multiple TFs (Szemenyei *et al.*, 2008; Causier *et al.*, 2012) and inhibitors of hormone signaling (Pauwels *et al.*, 2010; Ke *et al.*, 2015; Ma *et al.*, 2017; Martin-Arevalillo *et al.*, 2017; Kuhn *et al.*, 2020). Interactions with EAR motifs enable the recruitment of TPL/TPRs into oligomers and complexes with histones, potentially reducing access of TFs to DNA (Ma *et al.*, 2017; Martin-Arevalillo *et al.*, 2017). The N-terminal domain in *Arabidopsis* TPL further contributes to an oligomerization-independent mode of corepression, likely preventing the engagement of mediator subunits into active transcription complexes (Leydon *et al.*, 2021). TPL/TPRs also interact with histone deacetylases, providing a mechanism for repression of gene expression by interfering with a transcription-permissive chromatin state (Long *et al.*, 2006; Zhu *et al.*, 2010; Leng *et al.*, 2020). Thus, several molecular mechanisms assist TPL/TPRs corepressor activity.

TPL/TPRs have been implicated in the regulation of plant immunity. First, oomycete and fungal effectors target TPL/TPRs to promote host susceptibility (Harvey *et al.*, 2020; Darino *et al.*, 2021). Second, mutating *TPL*, *TPR1*, and *TPR4* in *Arabidopsis* or silencing of *TPR1* in *Nicotiana benthamiana* compromised TNL receptor signaling and an flg22 PAMP-triggered reactive oxygen species (ROS) burst (Zhu *et al.*, 2010; Zhang *et al.*, 2019; Navarrete *et al.*, 2021). By contrast, *Arabidopsis TPR2* and *TPR3* were identified as negative regulators of TNL Suppressor of Nonexpressor of Pathogenesis-related 1 (NPR1) Constitutive 1 (SNC1)-conditioned autoimmunity (Garner *et al.*, 2021). *Arabidopsis* TPR1 is associated with promoters of genes that are downregulated in $TNL^{RRS1\text{-}RPS4}$ ETI (Bartsch *et al.*, 2006; Zhu *et al.*, 2010) and represses the expression of cyclic nucleotide-gated channel (*CNGC*) genes also known as *Defense No Death 1* and *2* (*DND1/CNGC2* and *DND2/CNGC4*; Zhu *et al.*, 2010; Niu *et al.*, 2019). Since these *dnd* mutants show enhanced bacterial resistance (Clough *et al.*, 2000; Jurkowski *et al.*, 2004), a picture emerged in which TPR1 promotes TNL ETI by limiting the expression of negative regulators of defense (Zhu *et al.*, 2010). However, the lack of a genome-wide profile of TPL/TPR chromatin associations leaves other functions of these corepressors in defense signaling unclear.

Here, using chromatin immunoprecipitation with sequencing (ChIP-Seq), we examined genome-wide TPR1-chromatin associations conditional on *EDS1*-controlled immunity in *Arabidopsis* lines expressing *pTPR1:TPR1-GFP*. We further examined RNA expression profiles and physiological phenotypes of wild-type and *tpr1 tpl tpr4* (*t3*) mutant plants during bacterial infection. Taken together, our data suggest that TPL/TPR transcriptional corepressors operate at the chromatin not only to assist in the restriction of pathogen growth but also to mitigate deleterious effects of induced immunity on plant health.

Materials and Methods

Plant materials and growth conditions

Arabidopsis thaliana (L.) *Heynh.* accession Col-0 *tpr1* single mutant, *tpr1 tpl tpr4* (*t3*) triple mutant, *pTPR1:TPR1-GFP* Col-0 (*TPR1* Col), and *pTPR1:TPR1-HA* Col-0 stable transgenic lines were described previously (Zhu *et al.*, 2010). *pTPR1:TPR1-GFP eds1-2* (*TPR1 eds1*) and *pTPR1:TPR1-GFP sid2-1* (*TPR1 sid2*) lines were generated by crossing *TPR1* Col (Zhu *et al.*, 2010) with Col-0 *eds1-2* (Bartsch *et al.*, 2006) and Col-0 *sid2-1* (Wildermuth *et al.*, 2001), respectively. Complementation *tpr1 tpl tpr4 pTPR1:TPR1-GFP* lines were generated by floral dipping of *t3* with Agrobacteria GV3101 pMP90 pSoup carrying *pCAMBIA1305-TPR1-GFP* (Zhu *et al.*, 2010). The *coi1-41* mutant is described in Cui *et al.* (2018). The mutant *eds1-2* (Bartsch *et al.*, 2006) was used throughout the study, with the exception of root growth inhibition and MAPK assays, where the *eds1-12* line (Ordon *et al.*, 2017) was used. The mutant *eds1-12 pad4-1 sag101-3* (*eps*) is described in Ordon *et al.* (2017) and Pruitt *et al.* (2021). The *fls2* (SAIL_691C4), *rlp23-1*, and *pepr1-1 pepr2-3* mutants are described earlier (Zipfel *et al.*, 2004; Krol *et al.*, 2010; Albert *et al.*, 2015). Oligonucleotides for genotyping are shown in Supporting Information Table S1. For bacterial infection assays, plants were grown under a 10 h light period (*c.* 100 μmol m^{-2} s^{-1}) and 22°C : 20°C, day : night temperature regime with 60% relative humidity. For transformation and selection of combinatorial mutants, plants were grown under

22 h light (*c.* 100 μmol m^{-2} s^{-1}) and a 22°C : 20°C, day : night temperature regime with 60% relative humidity.

Immunoblot analyses

For immunoblotting of TPR1-GFP, total protein extracts were prepared by incubating liquid nitrogen-ground samples (*c.* 50 mg) in 2× Laemmli loading buffer for 10 min at 95°C. Samples were centrifuged for 1 min at 10 000 ***g*** to remove cell debris before gel loading. Proteins were separated by 10% (v/w) SDS-PAGE (1610156; Bio-Rad, Hercules, CA, USA) and transferred to a nitrocellulose membrane (0600001; GE Healthcare Life Sciences, Chicago, IL, USA). α-GFP antibodies (no. 2956; Cell Signaling Technology, Danvers, MA, USA, or no. 11814460001; Roche, Basel, Switzerland) in combination with HRP-conjugated anti-rabbit or anti-mouse secondary antibodies (A9044 or A6154; Merck, Darmstadt, Germany) were used. In MAPK3/6 phosphorylation assays, seedlings were treated for 15 and 180 min with pep1 or milliQ water (mQ, mock) as a negative control. Proteins were extracted with a buffer containing 50 mM Tris pH 7.5, 200 mM NaCl, 1 mM EDTA, 10 mM NaF, 2 mM sodium orthovanadate, 1 mM sodium molybdate, 10% (v/v) glycerol, 1 mM AEBSF, 0.1% Tween-20, 1 mM dithiothreitol, 1× protease inhibitor cocktail (11836170001; Roche), and 1× phosphatase inhibitor cocktail (4906845001; Roche). Extracts were resolved on 8% (v/w) SDS-PAGE (1610156; Bio-Rad) and transferred onto a nitrocellulose membrane (0600001; GE Healthcare Life Sciences). Primary antibody against phospho-p44/42 MAP kinase (#9101; Cell Signaling Technologies) was used in combination with HRP-conjugated anti-rabbit as a secondary antibody (A6154; Merck). Signal detection was performed using Clarity and Clarity Max luminescence assays (1705061 and 1705062; Bio-Rad). For loading control, membranes were stained with Ponceau S (09276-6X1EA-F; Merck).

Salicylic acid quantification

Quantification of free SA was done as described (Straus *et al.*, 2010) with a chloroform/methanol/water extraction containing SA-d_4 (CS04-482_248; Campro Scientific, Berlin, Germany) as internal standard. After phase extraction, drying of polar phase, dissolving in sodium acetate (pH 5.0), uptake in ethyl acetate : hexane (3 : 1), and derivatization, 1 μl sample was injected into a gas chromatograph coupled to a mass spectrometer (GC–MS; Agilent, Santa Clara, CA, USA) on an HP-5MS column (Agilent). Masses of SA-d_4 (*m/z* 271) and SA (*m/z* 267) were detected by selected ion monitoring and quantified using the CHEMSTATION software (Agilent).

Chl*a* fluorescence and chlorophyll quantification

Maximum quantum efficiency (F_v/F_m) of photosystem II (PSII) and the effective efficiency (φPSII) in Col, *tpr1*, *t3*, and *eds1* leaves were determined after syringe infiltration of *Pst* (OD_{600} = 0.005) by Chl*a* fluorescence analysis using a MINI-PAM fluorimeter (Walz, Effeltrich, Germany). Measurements of three to four leaves from independent plants were performed at each timepoint in a randomized and rotating order between 13:00 and 15:00 h on Days 0–4 after inoculation (10:00–11:00 h). Mock (10 mM $MgCl_2$)-infiltrated leaves from different plants were measured as controls. To determine the maximum quantum yield ($F_v/F_m = (F_m - F_0)/F_m$; Baker, 2008), plants were first dark-acclimated for 20 min. The operating PSII efficiency of photosystem II (φPSII = $(F_m' - F)/F_m'$; Baker, 2008) was determined with 12 saturating light flashes (*c.* 1300 μmol photons m^{-2} s^{-1}) at intervals of 20 s under actinic light intensity of *c.* 216 μmol photons m^{-2} s^{-1}. Data from three independent experiments were combined, statistically analyzed using ANOVA and Tukey's HSD test (α = 0.05), and plotted using the 'ggline' function in the 'GGPUBR' R package. In Chl*a* fluorescence assays with nlp24 treatment, nlp24 (AIMYAWYFPKDSPM LLMGHRHDWE, crude peptide; Genscript, Piscataway, NJ, USA; dissolved in DMSO) was applied by leaf infiltration at a final concentration of 5 μM (10 mM $MgCl_2$, 0.05% DMSO). Data from four independent experiments were combined and statistically analyzed using ANOVA and Tukey's HSD test (α = 0.05). Total leaf chlorophyll (*a* + *b*) contents were determined at 3 d after syringe infiltration with *P. syringae* pv *tomato* DC3000 bacteria (OD_{600} = 0.005) or mock (10 mM $MgCl_2$) treatment. The chlorophyll content in each sample was calculated as a mean of three leaf disks (diameter 8 mm) and analyzed according to Porra *et al.* (1989). Three independent experiments were performed and pooled for the statistical analysis keeping experiment as a factor in the ANOVA model (Tukey's HSD α = 0.05; *n* = 15).

Root growth inhibition assay

Root growth inhibition assays with pep1 and flg22 were performed as described (Igarashi *et al.*, 2012), with adjustments. Seeds were surface-sterilized and transferred into 48-well plates (one seed per well). Each well was supplied with 200 μl of 0.5× MS (including vitamins and MES, pH 5.4; M0255; Duchefa Biochemie, Haarlem, the Netherlands) and 5% (w/v) sucrose. flg22 (RP19986; GenScript) and *At*pep1 (referred to as pep1 in this study; ATKVKAKQRGKEKVSSGRPGQHN; GenScript) peptides were dissolved and administered as solutions in mQ water (final concentrations: flg22 – 100 nM, pep1 – 50 or 200 nM). Sterile mQ was added as a mock control. Root length was measured at 10 d using IMAGEJ software. Root growth inhibition (RGI) index was quantified as a ratio of the root length in flg22 or pep1 treatment to the mean of mock-treated plants. Data from independent experiments were combined and statistically analyzed using ANOVA (experiment as a factor) and Tukey's HSD test.

Details on the TPR1-GFP ChIP- and RNA-Seq procedures and data analysis, as well as other assays, are in Methods S1.

Results

Arabidopsis TPR1 Col displays constitutive transcriptional immunity

To investigate the role of TPR1 in plant immunity, we used an *Arabidopsis* Col-0 line expressing *TPR1-GFP* under control of its

2 kb upstream sequence (*pTPR1:TPR1-GFP*; hereafter *TPR1* Col) and displaying *EDS1*- and TNL *SNC1*-dependent constitutive immunity and SA accumulation (Zhu *et al.*, 2010). We introduced a null *eds1* (*eds1-2*) or *ics1* (*sid2-1*) mutation into *TPR1* Col to test TPR1-GFP functions without *EDS1*- or *ICS1*/SA-dependent signaling (Wildermuth *et al.*, 2001; Bartsch *et al.*, 2006). While TPR1-GFP accumulation was similar in all three lines (Fig. 1a), stunting of 5-6-wk-old *TPR1* Col plants was reduced in *TPR1 eds1* but not in *TPR1 sid2* (Zhu *et al.*, 2010; Figs 1b, S1a). Enhanced resistance of *TPR1* Col to virulent *P. syringae* pv *tomato* DC3000 (*Pst*) bacteria (Zhu *et al.*, 2010) was abolished in *TPR1 eds1* and partially compromised in *TPR1 sid2* plants (Zhu *et al.*, 2010; Fig. S1b). *TPR1 eds1* and *TPR1 sid2* plants had *c.* sevenfold lower SA levels than *TPR1* Col (Fig. S1c). These results suggest that constitutive defense in *TPR1* Col is mediated primarily by an SA-independent branch of *EDS1* signaling, consistent with *TPR1* Col autoimmunity involving TNL *SNC1* (Zhu *et al.*, 2010), which promotes SA-independent signaling (Zhang *et al.*, 2003; Zhu *et al.*, 2010).

RNA-Seq analysis of 5–6-wk-old *TPR1* Col, *TPR1 sid2*, *TPR1 eds1*, and wild-type Col plants showed that *EDS1* signaling impacted 61% of genes that are differentially expressed between *TPR1* Col and Col (Table S2; 942/1549, $|\log_2 FC| \geq 2$, FDR ≤ 0.05; Fig. S1d). By contrast, the *sid2* mutation affected the expression of *c.* 10% differentially expressed genes (DEGs; Table S2; 153/1549,$|\log_2 FC| \geq 2$, FDR ≤ 0.05). The 2194 DEGs between Col, *TPR1* Col, *TPR1 sid2*, and *TPR1 eds1* fell into 13 groups in hierarchical clustering of $\log_2$-transformed gene expression changes relative to Col (Fig. 1c; Table S3). Clusters 8 and 9 were skipped because their small size (< 20 genes) could affect the validity of statistical tests, but they are shown in Table S3. Cluster #1, with 524 genes induced in a *TPR1*/*EDS1*-dependent manner, was strongly enriched for Gene Ontology (GO) terms linked to *EDS1*- and SA-dependent immune responses (Fig. 1c; Table S4). By contrast, cluster #10, with 394 genes suppressed in *TPR1* Col (Fig. 1c), was enriched for genes linked to microtubule-based dynamics and cell cycle regulation (Table S4). These data show that TPR1-GFP constitutive immunity involves *EDS1*-dependent transcriptional reprogramming.

We tested whether the *TPR1* Col transcriptome aligns with gene expression profiles of PTI and ETI. For this, we cross-referenced DEGs from the 13 clusters above (Fig. 1c; Tables S2, S3) with RNA-Seq datasets for (1) Col inoculated with *Pst avrRps4* triggering an $ETI^{RRS1\text{-}RPS4}$ (Bhandari *et al.*, 2019) and (2) Col treated with the bacterial PAMP flg22 (Birkenbihl *et al.*, 2017; Figs 1d, S1e). Genes in clusters 1, 3, 4, 6, and 7 that were upregulated in *TPR1* Col vs Col (Fig. 1c) were also induced by *Pst avrRps4* or flg22 treatments (Fig. 1d). Similarly, repressed clusters in *TPR1* Col (#10, #11, Fig. 1c) were downregulated by these treatments (Fig. 1d). Accordingly, there was a significant overlap of DEGs induced in *TPR1* Col and treatments with flg22 or *Pst avrRps4* (Fig. 1e, Fisher's exact test $P < 0.05$). We concluded that the *TPR1* Col line displays constitutive transcriptional immunity and that *TPR1* Col and *TPR1 eds1* are suitable backgrounds to measure immunity-dependent and immunity-independent TPR1-chromatin associations.

TPR1 binds to promoters of genes upregulated in immunity activated tissues

We performed a ChIP-Seq analysis on leaves of 5–6-wk-old *TPR1* Col and *TPR1 eds1* plants (Fig. 2; Methods S1) using an input control for peak calling. A line expressing *pTPR1:TPR1-HA* in Col, which has a similar constitutive immunity phenotype as *TPR1* Col (Zhu *et al.*, 2010), was included as an additional control for peak calling. In *TPR1* Col, 1531 TPR1-GFP chromatin binding sites corresponded to 1441 genes (Table S5). Most peaks (723/1531, 47%) mapped to 1-kb upstream gene sequences as indicated by a metaplot analysis (Table S5; Fig. 2a,b). The results are consistent with TPR1 acting as a transcriptional corepressor at the promoters of *CNGC2* and *CNGC4* (Niu *et al.*, 2019). TPR1-bound genes showed enrichment of GO terms linked to defense and SA signaling as well as developmental processes (Table S6, FDR ≤ 0.05; Figs S2–S4), as expected from the *TPR1* Col enhanced defense and perturbed growth phenotypes (Fig. 1b,c).

In *TPR1 eds1*, which lacks constitutive immunity (Figs 1b,c, S1), we detected 614 TPR1-GFP-binding sites corresponding to 623 genes (Table S7; Fig. 2c). While the reduced number of peaks in TPR1 *eds1* did not affect TPR1 distribution across genomic fractions relative to *TPR1* Col (Fig. 2b,c; Table S7), the proportion of defense-related GO terms enriched among TPR1-GFP-bound genes plummeted in *TPR1 eds1* relative to *TPR1* Col (Table S8). Hence, TPR1-chromatin association with defense-related genes is likely enhanced in immune-activated shoot tissues. To assess this further, we compared TPR1-chromatin associations in *TPR1* Col and *TPR1 eds1* using a peak calling-independent method implemented in diffReps (Shen *et al.*, 2013). This analysis showed that TPR1-GFP enrichment was stronger in *TPR1* Col relative to *TPR1 eds1* at 247 genes (*G*-test, 1.5 times difference, FDR ≤ 0.05; Table S9), supporting stronger TPR1 binding at these loci in immune-activated *TPR1* Col. No ChIP peaks were called for 150 (61%) of these genes in *TPR1 eds1* (Tables S5, S7). Notably, 66 of the 247 differentially TPR1-bound genes (27%), including *ICS1*, cysteine-rich receptor-like kinases, and *WRKY* TFs (Fig. S2), were more highly expressed in *TPR1* Col compared with *TPR1 eds1* (Table S2, $\log_2 FC \geq 1$, FDR ≤ 0.05; Fig. 2d). Only 10 genes from the above set of 247 (*c.* 4%) were downregulated in *TPR1* Col compared with *TPR1 eds1* (Table S2, $\log_2 FC \leq 1$, FDR ≤ 0.05; Fig. 2d). In summary, TPR1 binds to *c.* 1400 genes mainly at promoter regions and *c.* 11% of detected TPR1 binding (150/1441 genes) is conditional on *EDS1*-dependent immunity.

We further tested whether *EDS1*-dependent TPR1-chromatin associations correlate with transcriptional reprogramming during defense. The set of 247 genes with a stronger TPR1-GFP signal in *TPR1* Col vs *TPR1 eds1* (Tables S9, S10) was induced after treatments with PAMP flg22 or *Pst avrRps4* (Fig. 2e, boxplots with orange shadowing). Conversely, the expression of 74 genes with lower TPR1-GFP enrichment in *TPR1* Col vs *TPR1 eds1* (Tables S9, S10) was unaltered or reduced in these treatments (Fig. 2e, boxplots with green shadowing). Similarly, genes bound by TPR1-GFP in *TPR1* Col were specifically enriched for genes

New Phytologist

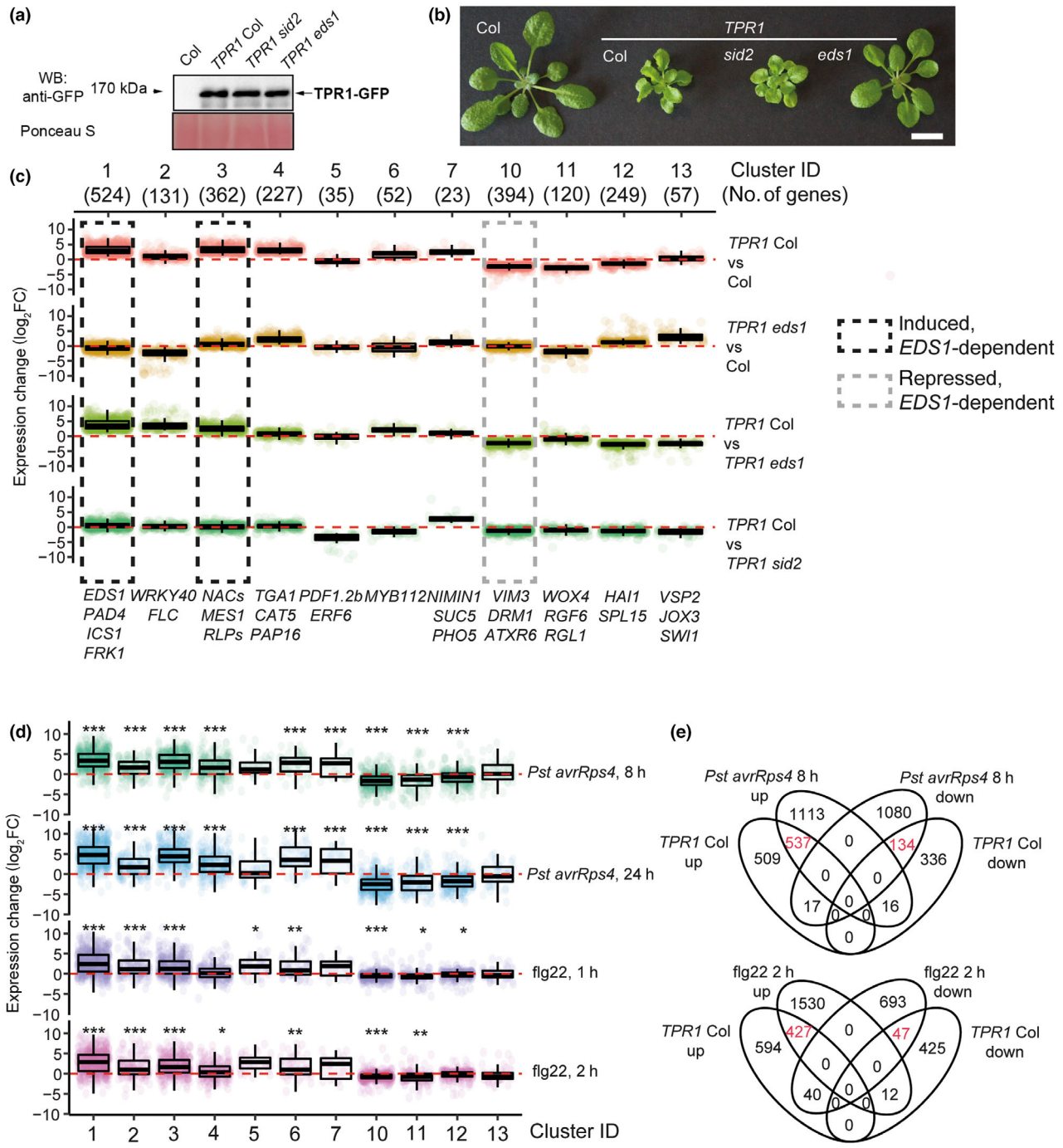

Fig. 1 Defense-related *EDS1*-dependent transcriptional reprogramming in *TPR1* Col line. (a) TPR1-GFP steady-state accumulation in 5–6-wk-old *Arabidopsis* Col-0 (Col), *sid2*, and *eds1* mutant plants expressing *pTPR1:TPR1-GFP* (*TPR1* Col, *TPR1 sid2*, and *TPR1 eds1*). The transgenic lines show similar levels of TPR1-GFP protein. Col was used as a negative control. Ponceau S staining indicates similar loading. The experiment was repeated three times with similar results. (b) Dwarfism in *TPR1* Col depends on functional *EDS1*. Col is shown on the left for comparison. Bar, 1 cm. (c) Log_2-transformed relative expression values of clusters of genes differentially expressed in Col, *TPR1 eds1*, and *TPR1 sid2* relative to *TPR1* Col or Col. Each dot corresponds to a single gene. Size of the cluster is given in parentheses. Genes in clusters 1 and 3 are upregulated (box with black dashed line) while cluster 10 (box with gray dashed line) is downregulated in an *EDS1*-dependent manner in *TPR1* Col relative to Col. Clusters 8 and 9 were skipped because their small size (< 20 genes) could affect validity of statistical tests, but they are shown in Supporting Information Table S3. Names of selected genes from the clusters are in italics. (d) Expression changes for genes in clusters from (c) in Col plants treated with *Pseudomonas syringae* pv *tomato* DC3000 *avrRps4* (*Pst avrRps4*) or flg22 at the indicated time points (Birkenbihl *et al*., 2017; Bhandari *et al*., 2019). The values are log_2-transformed fold changes (FC) relative to mock or untreated Col plants. Asterisks indicate that the mean log_2FC value in the cluster differs from 0 based on two-sided *t*-test followed by Bonferroni correction for multiple testing. *, $P < 0.05$; **, $P < 0.01$; ***, $P < 0.001$. (e) Venn diagrams showing the overlap between DEGs in *TPR1* Col (vs Col) and DEGs after flg22 and *Pst avrRps4*. Numbers are in red when Fisher's exact test shows statistically significant overlap ($P < 0.05$, Bonferroni correction).

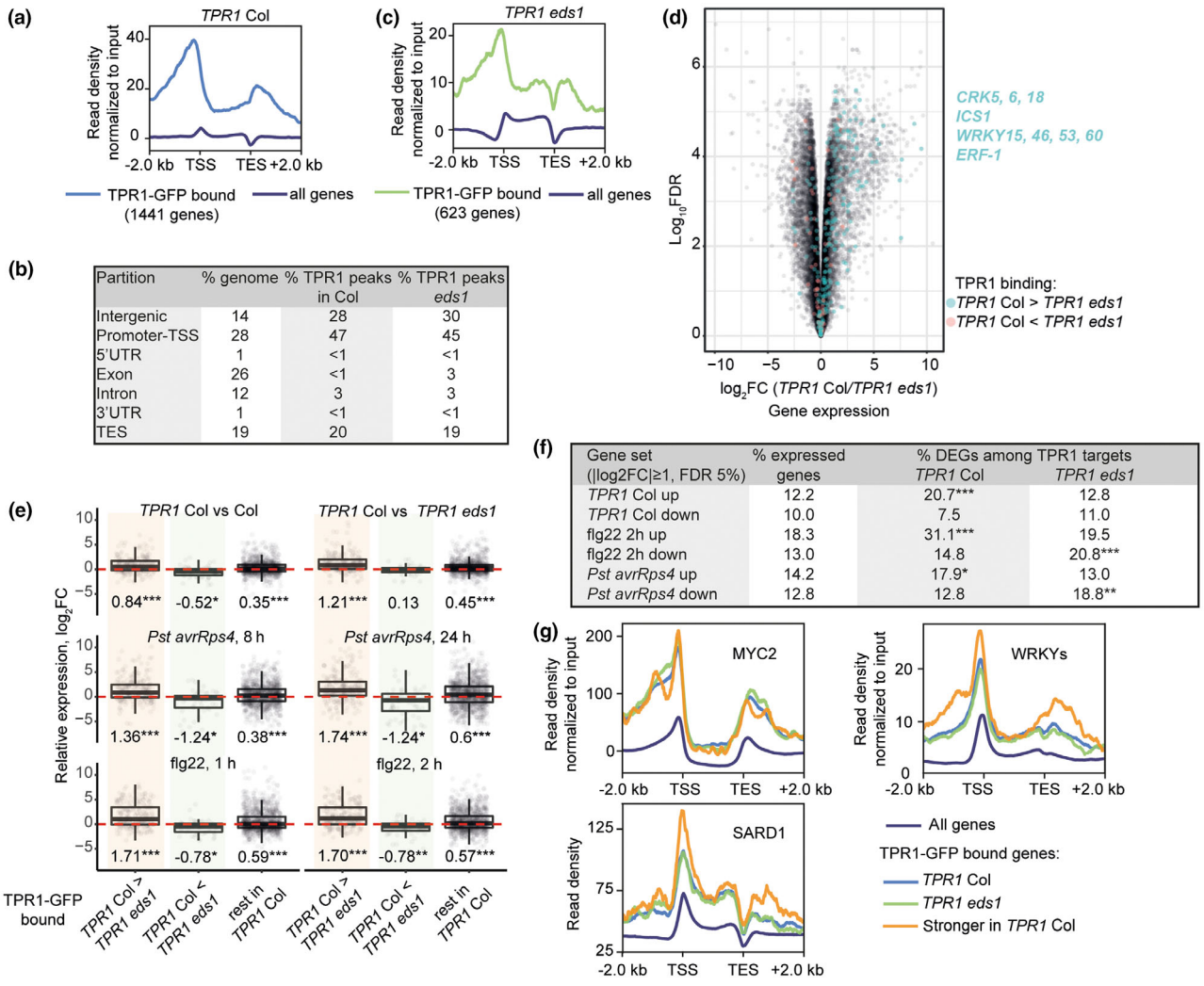

Partition	% genome	% TPR1 peaks in Col	% TPR1 peaks *eds1*
Intergenic	14	28	30
Promoter-TSS	28	47	45
5'UTR	1	<1	<1
Exon	26	<1	3
Intron	12	3	3
3'UTR	1	<1	<1
TES	19	20	19

(f)

Gene set (|log2FC|≥1, FDR 5%)	% expressed genes	% DEGs among TPR1 targets *TPR1* Col	*TPR1 eds1*
TPR1 Col up	12.2	20.7***	12.8
TPR1 Col down	10.0	7.5	11.0
flg22 2h up	18.3	31.1***	19.5
flg22 2h down	13.0	14.8	20.8***
Pst avrRps4 up	14.2	17.9*	13.0
Pst avrRps4 down	12.8	12.8	18.8**

Fig. 2 *Arabidopsis* TPR1-chromatin association partially depends on *EDS1*-controlled immune signaling. (a–c) Metaplots of ChIP-Seq TPR1-GFP enrichment profiles at the chromatin in *TPR1* Col (a) and *TPR1 eds1* (c) and distribution of TPR1 peaks over genome partitions (b). TPR1-GFP binds 1441 genes in *TPR1* Col and 623 genes in *TPR1 eds1*. The ChIP-Seq read density for TPR1-GFP was normalized to input via subtraction. The dark blue lines represent TPR1-GFP chromatin-binding profiles averaged across all annotated genes in Arabidopsis (TAIR10). TES, transcription end site; TSS, transcription start site. (d) Volcano plot displaying the relationship between *EDS1*-dependent TPR1-chromatin associations and the *EDS1*-dependent gene expression regulation in *TPR1* Col. Significance of difference in the TPR1-GFP enrichment in *TPR1* Col and *TPR1 eds1* was assessed with diffReps (≥1.5 times, *G*-test, FDR ≤ 0.05). Genes with stronger enrichment of TPR1-GFP in *TPR1* Col than in *TPR1 eds1* (blue dots) tend to have higher gene expression in *TPR1* Col. Selection of these genes is shown in blue text. (e) Log_2-scaled fold change of the relative expression of TPR1-GFP-bound genes in *TPR1* Col vs Col and *TPR1* Col vs *TPR1 eds1*, for treatment with *Pseudomonas syringae* pv *tomato* DC3000 (*Pst*) *avrRps4* (8 and 24 hpi vs 0 hpi) or flg22 (1 and 2 hpi vs 0 hpi) (Birkenbihl *et al*., 2017; Bhandari *et al*., 2019). Boxplots for genes showing stronger TPR1-GFP enrichment in *TPR1* Col vs *TPR1 eds1* (shown as 'TPR1 Col > TPR1 *eds1*', $n = 247$) are shaded in orange. Green shadowing marks a set of genes with weaker TPR1-GFP signal in *TPR1* Col vs *TPR1 eds1* ('TPR1 Col < TPR1 *eds1*', $n = 74$). Categorization is based on the diffRep results ($log_2|G| > 0.58$ or 1.5 times difference at $P\_adj \leq 0.05$. Genes that do not fall in these two categories are denoted as 'rest in *TPR1* Col' ($n = 1253$). The total number of genes in (e) 1574 differs from 1441 in (a) because diffReps works independently of peak calling while annotations in (a) are based on the peak calling. Genes with higher TPR1-GFP enrichment in *TPR1* Col show transcriptional upregulation after flg22 and *Pst avrRps4* treatments. Numbers below boxplots indicate mean log_2FC; its difference from 0 was assessed with two-sided *t*-test; Bonferroni-corrected *P*-values: *, $P < 0.05$; **, $P < 0.01$; ***, $P < 0.001$. Elements of boxplots: first quartile – minima, third quartile – maxima, median – central line; whiskers extend to the minimum and maximum values but not further than 1.5 interquartile range from the respective minima or maxima of the boxplot. Each dot represents a gene. (f) TPR1-GFP-associated loci in *TPR1* Col are enriched for genes upregulated in *TPR1* Col, after treatments with flg22 (2 h) and *Pst avrRps4* (8 h) (same as in e). Fisher's exact test *P*-value after Bonferroni correction: *, $P < 0.05$; **, $P < 0.01$; ***, $P < 0.001$. Number of expressed genes depends on the threshold applied during the differential gene expression analysis to remove low-expressed genes (*TPR1* Col – 18 884 genes; flg22 – 21 098; *Pst avrRps4* – 20 573). (g) Distribution of ChIP-Seq signal for MYC2 (Wang *et al*., 2019), WRKY (Birkenbihl *et al*., 2018), and SARD1 (Sun *et al*., 2015) transcription factors (TFs) across genes bound by TPR1-GFP in *TPR1* Col (light blue), *TPR1 eds1* (green) and genes bound stronger by TPR1-GFP in *TPR1* Col than in *TPR1 eds1* (orange). TF-chromatin binding profiles averaged across all annotated genes in Arabidopsis genome (dark blue) serve as a baseline. MYC2, WRKY TFs, and SARD1 are strongly enriched in promoters of genes bound by TPR1-GFP in *TPR1* Col and *TPR1 eds1*. ChIP-Seq data for SARD1 (Sun *et al*., 2015) did not have input samples and therefore were not normalized, but specificity of SARD1 binding was demonstrated in the original study. ChIP-Seq for MYC2 (Wang *et al*., 2019) and WRKY TFs (Birkenbihl *et al*., 2018) were normalized to the input via subtraction.

upregulated in *TPR1* Col (compared with Col) and in response to flg22 or *Pst avrRps4* (Fig. 2f; Table S11). Together, these observations suggest *EDS1*-dependent TPR1 binding to a set of genes that are upregulated in PTI and ETI.

TPR1 ChIP-Seq identifies known TPR1 and TPL targets

We detected TPR1-GFP enrichment at nine of 12 downregulated genes in $TNL^{RRS1\text{-}RPS4}$ ETI (Fig. S3) that were identified as TPR1-bound targets in a previous ChIP-qPCR study using the *TPR1-HA* Col transgenic line (Zhu *et al.*, 2010). Genes with TPR1-GFP enrichment include *DND1* and *DND2* (Fig. S3) encoding CNGC2 and 4, respectively, which are required for calcium-dependent immunity responses in PTI and ETI (Clough *et al.*, 2000; Jurkowski *et al.*, 2004; Tian *et al.*, 2019). TPR1-GFP binding at these loci was not obviously altered in *TPR1 eds1* (Fig. S3), indicating immunity status-independent association of TPR1 with promoters of these nine genes. Since TPL/TPRs have redundant functions (Zhu *et al.*, 2010; Harvey *et al.*, 2020; Plant *et al.*, 2021), we expected overlap in binding targets between TPL and TPR1. Indeed, TPR1-GFP was enriched at several TPL targets found with ChIP-qPCR such as *Constans* (Goralogia *et al.*, 2017), *Apetala 3* (Gorham *et al.*, 2018), *Circadian clock associated 1*, *Leafy*, and others (Lee *et al.*, 2020) in both *TPR1* Col and *TPR1 eds1* (Fig. S4). Hence, our TPR1-GFP ChIP-Seq profiles provide a genome-wide resource for identifying TPL/TPR chromatin targets.

TPR1 shares binding targets with MYC2, SARD1 and WRKY TFs

The genome-wide profiles of TPR1-chromatin associations in immune-activated and nonactivated leaf tissues prompted us to investigate whether certain DNA motifs correlate with TPR1 binding. A *de novo* motif search revealed strong enrichment of the GAGA motif (C-box) under TPR1 peaks in *TPR1* Col and *TPR1 eds1* (Fig. S5a). The G-box (CACGTG) bound by MYC2 and other bHLH TFs was also over-represented under TPR1-GFP peaks in *TPR1 eds1* (Fig. S5a). We validated this signature by reanalyzing published MYC2 ChIP-Seq profiles (Figs 2g, S5b). A MYC2 ChIP signal (Wang *et al.*, 2019) was similarly enriched at promoters of genes bound by TPR1-GFP in *TPR1* Col and *TPR1 eds1* (Fig. 2g). Also, TPR1-bound genes showed statistically significant enrichment of reported MYC2 targets (Van Moerkercke *et al.*, 2019; Zander *et al.*, 2020; Fig. S5b). Our *de novo* motif searches did not find evidence for the enrichment of W-box 'TTGACY' bound by WRKYs (Ciolkowski *et al.*, 2008) or the 'GAAATTT' element bound by SARD1 (Sun *et al.*, 2015). Considering the importance of these TFs in immune responses, we specifically examined the distribution of WRKY and SARD1 TFs binding at TPR1-GFP-bound genes using available ChIP-Seq data (Sun *et al.*, 2015; Birkenbihl *et al.*, 2018; Figs 2g, S5c,d). The metaplot and enrichment analyses for sets of genes associated with TPR1-GFP and TF peaks revealed that WRKY TFs and SARD1 binding sites strongly overlap with those for TPR1-GFP (Figs 2g, S5c,d). These results suggest that TPR1 shares some *in vivo* binding targets with MYC2, SARD1, and WRKY TFs.

TPL/TPRs suppress prolonged expression of $TNL^{RRS1\text{-}RPS4}$ ETI-induced genes

To explore the functions of TPR1 and other TPL/TPRs in pathogen defense, we infiltrated *Arabidopsis tpr1* single and *tpr1 tpl tpr4* triple (*t3*) mutants with avirulent ($TNL^{RRS1\text{-}RPS4}$-inducing) *Pst avrRps4* or virulent *Pst* (EV) bacteria alongside Col and hyper-susceptible Col *eds1-2* (*eds1*). As expected for ETI, Col showed stronger restriction of *Pst avrRps4* than *Pst* growth (0.7 $\log_{10}$; Tukey's HSD $P = 0.00007$) (Fig. 3a,b). The difference in colony-forming units (CFU) counts is similar to earlier studies from our laboratory (Lapin *et al.*, 2019; Sun *et al.*, 2021) but lower than in other studies (Saucet *et al.*, 2015; Ngou *et al.*, 2021), suggesting that experimental conditions (e.g. humidity) influence absolute differences in CFU of these strains in Col. Growth of *Pst avrRps4* and *Pst* in *tpr1* was not different from Col, and *t3* had two- to threefold increased CFU counts at 3 d (0.3–0.4 on $\log_{10}$ scale, $P = 0.277$ and 0.026 in assays with *Pst avrRps4* and *Pst*, respectively; Fig. 3a,b).

Arabidopsis TPL represses MYC2 (Pauwels *et al.*, 2010) which, when activated by bacterial coronatine, antagonizes *EDS1*- and *ICS1*/SA-dependent bacterial resistance (Zheng *et al.*, 2012; Cui *et al.*, 2018; Bhandari *et al.*, 2019). We therefore tested whether defects of *tpr1* and *t3* mutants in bacterial resistance are masked by coronatine. For that, *tpr1* and *t3* plants were infiltrated with coronatine-deficient *Pst Δcor avrRps4* or *Pst Δcor* (Fig. 3c,d). A mutant of the coronatine insensitive 1 (COI1) JA coreceptor was included as a negative control (Zheng *et al.*, 2012). In line with earlier studies, Col displayed bacterial coronatine-dependent susceptibility compared with *coi1* (Fig. 3b,d), and *Pst* coronatine-promoted virulence was no longer detected in avrRps4-activated $TNL^{RRS1\text{-}RPS4}$ ETI (Cui *et al.*, 2018; Bhandari *et al.*, 2019; Fig. 3a,b,d). These results confirm that $TNL^{RRS1\text{-}RPS4}$ ETI was functional in our assays. In the absence of coronatine, differences in bacterial growth between Col and the *t3* mutant increased to 0.5–0.6 on $\log_{10}$ scale ($P = 0.012$ and 0.0002 for *Pst Δcor avrRps4* or *Pst Δcor*, respectively; Fig. 3c,d). We concluded that TPR1/TPL contribute to *Arabidopsis* basal resistance and ETI against *Pst* (Zhu *et al.*, 2010), but this is largely masked by bacterial coronatine virulence.

We performed RNA-Seq on leaves of the *tpr1* and *t3* mutants alongside Col and *eds1* using *Pst avrRps4* since the timing of major *EDS1*-dependent transcriptional reprogramming between 4 and 24 hpi is well established for this strain (Bhandari *et al.*, 2019; Saile *et al.*, 2020; Sun *et al.*, 2021). Leaves of 5–6-wk-old plants were infiltrated with *Pst avrRps4* and samples collected at 0 (*c.* 5 min), 8, and 24 hpi (Table S12). As expected, the number of transcriptionally induced genes was higher in Col compared with *eds1* at 8 (2097 genes) and 24 (1289 genes) hpi (Table S12, $\log_2 FC \geq 1$, $FDR \leq 0.05$). Surprisingly, only one DEG was detected between Col and *tpr1* or *t3* mutants at these time points (Table S12, $|\log_2 FC| \geq 1$, $FDR \leq 0.05$). This was a gene of

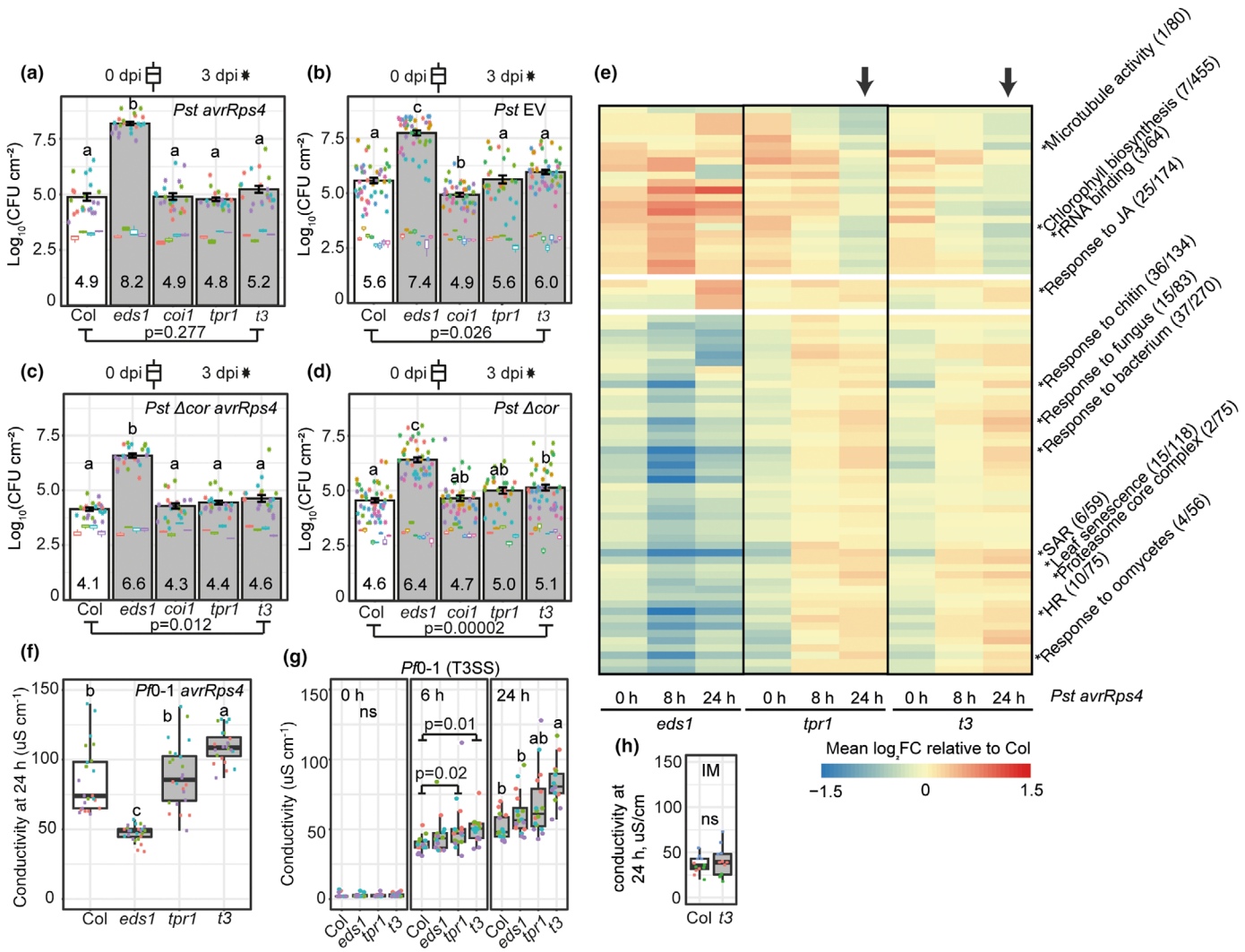

Fig. 3 *Arabidopsis TPL/TPRs* have a dual role during bacterial resistance responses. (a–d) Titers of *Pseudomonas syringae* pv *tomato* DC3000 (*Pst*) *avrRps4* (a), *Pst* (b), *Pst avrRps4 Δcor* (c), *Pst Δcor* (d) bacteria in indicated *Arabidopsis* mutants relative to Col plants (3 d after syringe infiltration, 3 d post-inoculation (dpi), $OD_{600} = 0.001$). *eds1* mutant served as a susceptibility control, and the *coi1* mutant – as a readout for the coronatine-promoted susceptibility. The *tpr1 tpl tpr4* (*t3*) mutant showed higher, but not significantly increased levels of the *Pst avrRps4* and *Pst* growth compared with Col (Tukey's HSD, $\alpha = 0.001$; $n = 22$ from four independent experiments with *Pst avrRps4* and $n = 46$ from eight independent experiments with *Pst*). *Pst* grows to higher densities than *Pst avrRps4*, *Pst Δcor*, or *Pst Δcor avrRps4* in Col plants (codes from Tukey's HSD test at $\alpha = 0.001$ are a, c, bc, b, respectively). Mean $\log_{10}$ CFU values are given for each genotype inside the bar. Error bars represent SEM. Experiments shown in (a–d) were performed alongside each other. (e) Heatmap of mean expression values for genes associated with selected GO terms in indicated mutants relative to Col after syringe infiltration of *Pst avrRps4* ($OD_{600} = 0.005$). Shown GO terms were differentially expressed in one of the genotypes relative to Col ($|\log_2 FC| \geq 0.58$ or 1.5 times, *t*-test at FDR < 0.05, asterisk shows where the GO terms are on the heatmap). Numbers next to the names of GO terms are the number of TPR1-bound genes vs the total number of genes in the corresponding GO term. The *tpr1* and *t3* mutants displayed a significant increase in the expression of genes from defense-related GO terms at 24 h (black arrow), for example, 'systemic acquired resistance' (SAR) and 'response to bacterium'. The '0 h' time point refers to *c*. 5 min after the infiltration. (f, g) Electrolyte leakage in *Arabidopsis* plants of indicated genotypes in response to nonvirulent *Pseudomonas fluorescens* bacteria *Pf*0-1 equipped with type III secretion system (T3SS) and expressing (f) or not (g) the avrRps4 effector ($OD_{600} = 0.2$). The *t3* mutant displayed increased electrolyte leakage at 24 h postinfection with these strains (Tukey's HSD, $\alpha = 0.001$; $n = 16$ from four independent experiments). Smaller differences were also detected at 6 hpi in *tpr1* and *t3* treated with *Pf*0-1 (T3SS, $P < 0.05$) but not at 0 hpi (ANOVA, $P > 0.05$). (h) The differential electrolyte leakage response in *t3* is bacteria-triggered since infiltration of 10 mM $MgCl_2$ (infiltration medium, IM) gave similar conductivity levels in Col-0 and *t3* at 24 h (ANOVA, $P > 0.05$). ns, not significant; CFU, colony-forming units. Elements of boxplots and matching statistics: first quartile – minima, third quartile – maxima, median – central line; whiskers extend to the minimum and maximum values but not further than 1.5 interquartile range from the respective minima or maxima of the boxplot. Datapoints with the same color were recorded in one independent experiment. Non-overlapping lowercase letter combinations above the bars and boxplots indicate statistically significant differences between the samples (Tukey's HSD test at $\alpha = 0.001$).

unknown function, *Plastid transcriptionally active 17* (*PTAC17*, AT1G80480). We concluded that TPL/TPRs are largely dispensable for the transcriptional mobilization of defense in TNL$^{RRS1\text{-}RPS4}$-mediated ETI to *Pst* bacteria, probably reflecting their limited contribution to bacterial growth restriction under our experimental conditions (Fig. 3a–d).

We applied a more sensitive analysis to test whether functionally coherent gene groups rather than individual genes are differentially expressed in *tpr1* and *t3* immune responses. For this, we used GO-based grouping of genes considering only GOs with 50–2000 genes. 76 of 350 tested GO-based gene sets were differentially expressed in one of the mutant lines (*eds1*, *tpr1*, and *t3*) at 0, 8, or 24 h relative to Col, as shown in heatmaps (Figs 3e, S6a) and Table S13 ($|\log_2 FC| \geq 0.5$, FDR ≤ 0.01). At 0 hpi (*c.* 5 min after *Pst avrRps4* infiltration), *eds1*, *tpr1*, and *t3* had reduced expression of genes with GO terms 'systemic acquired resistance' and 'response to bacterium' (Figs 3e, S6a,b), probably reflecting defects in a general stress response to leaf infiltration (Fig. S6c; Bhandari *et al.*, 2019; Van Moerkercke *et al.*, 2019). At 8 hpi, *tpr1* and *t3* mutants were more similar to Col than *eds1* (Fig. S6a,b), underscoring the dispensability of TPL/TPRs for early transcriptional mobilization of resistance (Fig. 3e; Ding *et al.*, 2020). Strikingly, at 24 hpi gene sets corresponding to GO terms 'systemic acquired resistance' and 'response to bacterium' had elevated expression in *tpr1* and *t3* mutants compared with Col (for the whole GO term, mean $\log_2 FC = 0.26$–0.30, or *c.* 1.2 times, FDR < 0.05; Figs 3e, S6a,b). Eight other GO terms such as 'response to fungus', 'leaf senescence', 'proteasome complex', and 'exocyst' also showed upregulation in *tpr1* and *t3* mutants (for the whole GO term, mean $\log_2 FC \geq 0.29$ or ≥ 1.95 times in *t3*, FDR < 0.05, full data in Table S13). These results suggest that TPL/TPRs contribute to the repression of defense gene expression after the initial wave of transcriptional elevation in a $TNL^{RRS1\text{-}RPS4}$ ETI response. The transcriptome profiles of *tpr1* and *t3* in $TNL^{RRS1\text{-}RPS4}$ ETI suggest a complex role of TPL/TPRs in immunity depending on the stage of the immune response.

The *tpr1 tpl tpr4* mutant displays enhanced bacteria-triggered electrolyte leakage

Because several GO terms associated with immune responses were weakly upregulated in *tpr1* and *t3* at 24 hpi with *Pst avrRps4* (Fig. S6a; Table S13), we tested whether TPL/TPRs help to restrict activated immune responses. In $TNL^{RRS1\text{-}RPS4}$ ETI, host cell death measured as electrolyte leakage can be uncoupled from bacterial growth restriction (Heidrich *et al.*, 2011; Lapin *et al.*, 2019; Saile *et al.*, 2020). We quantified electrolyte leakage in *tpr1* and *t3* mutants after infiltration of the type III secretion system (T3SS) equipped *Pseudomonas fluorescens* (*Pf*) 0–1 strain delivering avrRps4. At 24 h after *Pf*0-1 *avrRps4* infiltration, conductivity was higher in Col than *eds1*, consistent with *EDS1* being essential for TNL-triggered cell death (Heidrich *et al.*, 2011; Lapin *et al.*, 2019; Saile *et al.*, 2020; Fig. 3f). While *tpr1* plants behaved similarly to Col, the *t3* mutant had increased conductivity at 24 hpi compared with Col (Fig. 3f). The same *Arabidopsis* lines were infiltrated with *Pf*0-1 empty vector (EV) that elicits strong PTI (Sohn *et al.*, 2014; Saile *et al.*, 2020). T3SS-equipped *Pf*0-1 (EV) also increased electrolyte leakage in the *t3* mutant at 24 and weakly at 6 hpi compared with Col plants (Fig. 3g). No differences in electrolyte leakage were found between Col and *t3* under mock treatment conditions (Fig. 3h). These observations suggest that the *t3* mutant is defective in limiting bacteria-triggered cell death or damage.

We generated three independent stable homozygous lines expressing *pTPR1:TPR1-GFP* in the *t3* background. None of them displayed *TPR1* Col-like growth retardation or high TPR1-GFP protein accumulation (Fig. 4a,b). Despite having different TPR1-GFP amounts, these lines displayed reduced electrolyte leakage similar to wild-type Col and lower than *t3* (L2 and L3) or at the intermediate level (L1) at 24 hpi *Pf*0-1 EV infiltration (Fig. 4c). These data suggest a role of TPR1 in limiting bacteria-triggered electrolyte leakage. We propose that one potentially important and hitherto unknown role of TPR1 and other TPL/TPRs is to prevent an over-reaction of host tissues to pathogen infection.

TPL/TPRs reduce physiological damage associated with prolonged immunity

Genes with GO terms related to chloroplast functions were more strongly downregulated in *tpr1* and *t3* relative to Col at 24 hpi with *Pst avrRps4* (Table S13). Also, TPR1-GFP was enriched at upstream sequences of *LHCA2* (light-harvesting complex gene 2) and nine other genes from these GO terms in *TPR1* Col (Fig. 5a; Table S13). Therefore, we hypothesized that TPR1 and other TPL/TPRs regulate photosynthetic performance during an immune response. We tested chlorophyll content and photosynthetic efficiency in healthy and bacteria-infected plants by quantifying photosystem II (PSII) fluorescence. While alterations in the operating PSII efficiency (φPSII) are measurable during short-term stress, a drop in the maximum quantum yield of PSII (F_v/F_m) reflects more acute damage to PSII, and is observed under prolonged stress conditions (Baker, 2008). The *tpr1* and *t3* mutants were infiltrated with *Pst* bacteria ($OD_{600} = 0.005$) or mock solution (10 mM $MgCl_2$) alongside Col and *eds1*, which shows enhanced disease symptoms with *Pst*. Total chlorophyll content was reduced to a similar extent in Col, *tpr1*, and *t3* upon *Pst* infection (Fig. 5b). A reduction in φPSII and F_v/F_m values was minimal in infected Col leaves over the course of 3 d, indicating that these plants effectively balance bacterial growth restriction and PSII activity (Fig. 5c,d; purple line). By contrast, *tpr1*, *t3*, and *eds1* had decreased φPSII and F_v/F_m over 3 d following *Pst* infection (Fig. 5b,c; orange line – *tpr1*, blue line – *t3*). Reduced φPSII and F_v/F_m in *t3* and *eds1* correlated with greater loss of fresh weight at 3 d after the *Pst* infiltration ($OD_{600} = 0.005$, Fig. 5e). These observations suggest a role of TPL/TPRs in maintaining crucial photosynthetic functions in *Pst*-infected leaves, although confounding effects of the increased bacterial growth in *t3* (Fig. 3a–d) cannot be excluded.

We used a pathogen-free system to test the role of TPL/TPRs in maintaining photosystem II functions upon activation of the immune system. PAMP nlp24 is recognized by the cell surface-localized receptor-like protein RLP23 (Oome *et al.*, 2014; Albert *et al.*, 2015; Seidl & Van den Ackerveken, 2019). RLP23 signals via the EDS1/PAD4 heterodimer in *Arabidopsis* (Pruitt *et al.*, 2021; Tian *et al.*, 2021). Although treatment with nlp24 did not alter F_v/F_m at 3 d (Fig. 5f), the operating PSII performance (φPSII) was reduced in Col in an *EDS1*-dependent

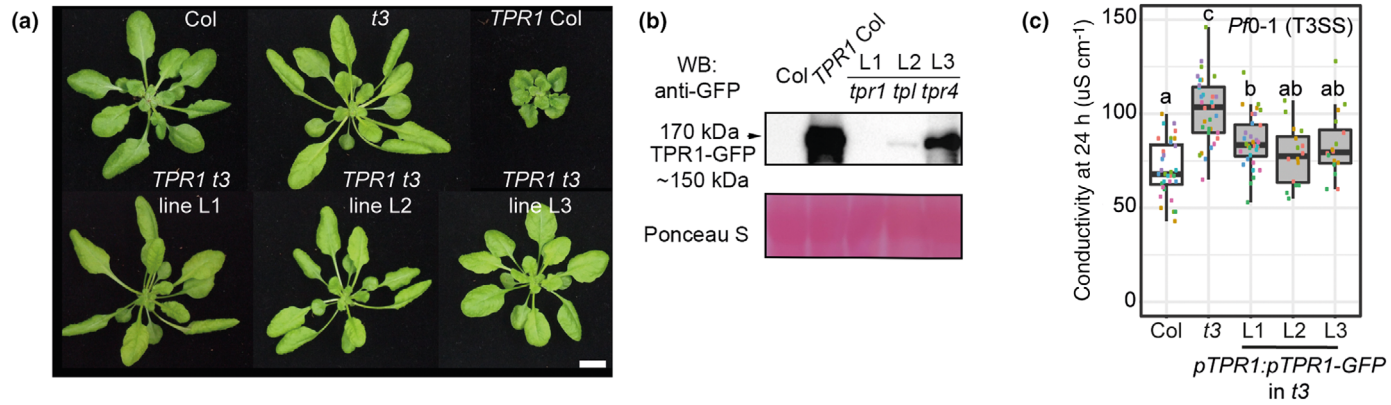

Fig. 4 *Arabidopsis* TPR1 counteracts electrolyte leakage triggered by the T3SS-equipped *Pf*0-1 bacteria. (a) Representative photographs of rosettes of 5–6-wk-old plants from three independent homozygous complementation lines expressing *pTPR1:TPR1-GFP* in *tpr1 tpl tpr4* (*t3*). *TPR1* Col is shown for comparison. The complementation lines do not show dwarfism in contrast to *TPR1* Col with the constitutive defense signaling. Scale bar = 1 cm. (b) Steady-state levels of TPR1-GFP in lines from (a), determined via Western blot analysis. Total protein extracts were probed with α-GFP antibodies. Ponceau S staining was used to control loading. The experiment was repeated two times with similar results. (c) Electrolyte leakage in the complementation lines from (a) and control lines Col and *t3* at 24 h after the *Pf*0-1 T3SS (OD_{600} = 0.2) infiltration. The complementation lines L1–L3 show a level of the electrolyte leakage comparable to Col (Tukey's HSD α = 0.001; different colors of data points correspond to independent experiments, *n* = 12–24 from three or six independent experiments). Elements of boxplots and matching statistics: first quartile – minima, third quartile – maxima, median – central line; whiskers extend to the minimum and maximum values but not further than 1.5 interquartile range from the respective minima or maxima of the boxplot. Datapoints with the same color were recorded in one independent experiment. Non-overlapping lowercase letter combinations above boxplots indicate statistically significant differences between the samples (Tukey's HSD α = 0.001).

manner (Fig. 5g). The nlp24-triggered φPSII reduction was stronger in *t3* than in Col or the *t3 pTPR1:TPR1-GFP* L3 complementation line (Fig. 5g). This difference cannot be explained by increased perception of nlp24 in *t3* since *t3* was less sensitive to this PAMP than Col as measured in reactive oxygen species (ROS) burst assays (Fig. 5h,i). These results demonstrate that TPR1 and likely other TPL/TPRs contribute to maintaining PSII function in *EDS1*-dependent immunity.

We used the bacterial PAMP flg22 or phytocytokine *At*pep1 (pep1 hereafter) to evaluate the effect of TPL/TPRs on the growth of immune-triggered plants in a pathogen-free system (Fig. 6). Root growth inhibition (RGI) was similar in Col, *tpr1*, and *t3* mutants in the presence of 100 nM flg22 (Fig. 6a,b), but it was more pronounced in the *t3* mutant on medium supplemented with 50 or 200 nM pep1 (Fig. 6c–e). RGI hypersensitivity of *t3* seedlings to pep1 was rescued in the *TPR1-GFP* complementation lines (Fig. 6c–e). Perception of pep1 was not altered in *t3* compared with Col at the level of pep1-induced phosphorylation of mitogen-activated protein kinase 3 and 6 (MPK3 and MPK6; Fig. 6f). Also, *t3* seedlings showed Col-like induction of PTI marker genes *FRK1* (FLG22-induced receptor-like kinase 1) and *WRKY30* at 1 h after the flg22 or pep1 treatment (Fig. 6g). Hence, TPR1 and most likely other TPL/TPRs reduce RGI in phytocytokine-stimulated sterile seedlings. Taken together, the data suggest that *Arabidopsis* TPR1 and other TPL/TPRs limit physiological and growth penalties associated with induced immunity.

Discussion

Timely activation of immune responses is essential for plant resistance to pathogens. How activated defenses are subsequently restricted to prevent damaging over-stimulation of tissues is less clear. Here, we present evidence that TPR1 and probably other TPL/TPR family transcriptional corepressors contribute to limiting host physiological damage and growth inhibition associated with induced immunity.

We obtained ChIP-Seq chromatin association profiles for *Arabidopsis* TPR1 with or without constitutive *EDS1*-dependent defense. TPR1-GFP bound primarily to upstream regions of *c.* 1400 genes, and *c.* 10% of these genes showed enhanced TPR1-GFP binding when *EDS1*-dependent immunity signaling was active (Fig. 2). TPR1-GFP association with regions immediately upstream of the transcription start site (TSS) is consistent with TPR1 interaction with TFs (Szemenyei *et al.*, 2008; Causier *et al.*, 2012) and with the location of predicted TF-binding sites close to the TSS (Yu *et al.*, 2016). Although TPR1-bound genes are strongly enriched for ChIP signals of MYC2 (Van Moerkercke *et al.*, 2019; Wang *et al.*, 2019; Zander *et al.*, 2020), WRKYs (Birkenbihl *et al.*, 2018), and SARD1 (Sun *et al.*, 2015) TFs (Fig. 2g), there is so far no reported evidence for complex formation between these TFs and TPR1 in plant tissues. TPR1-GFP-bound genes are enriched for GO terms associated with defense and control of growth and development (Tables S6, S8). Also, binding of TPR1 to chromatin correlated with transcriptional activation (Fig. 2). However, we cannot draw a conclusion about causality between TPR1 binding and the transcriptional output. Time series ChIP-Seq and RNA-Seq experiments with complementation lines would be useful to address this question. Because of redundancy between TPL/TPR members, we think that the processed input-normalized TPR1-GFP chromatin enrichment profiles for *TPR1* Col and *TPR1 eds1* provided here could help researchers identify chromatin interactions for TPL/TPRs (see Data availability section).

New Phytologist

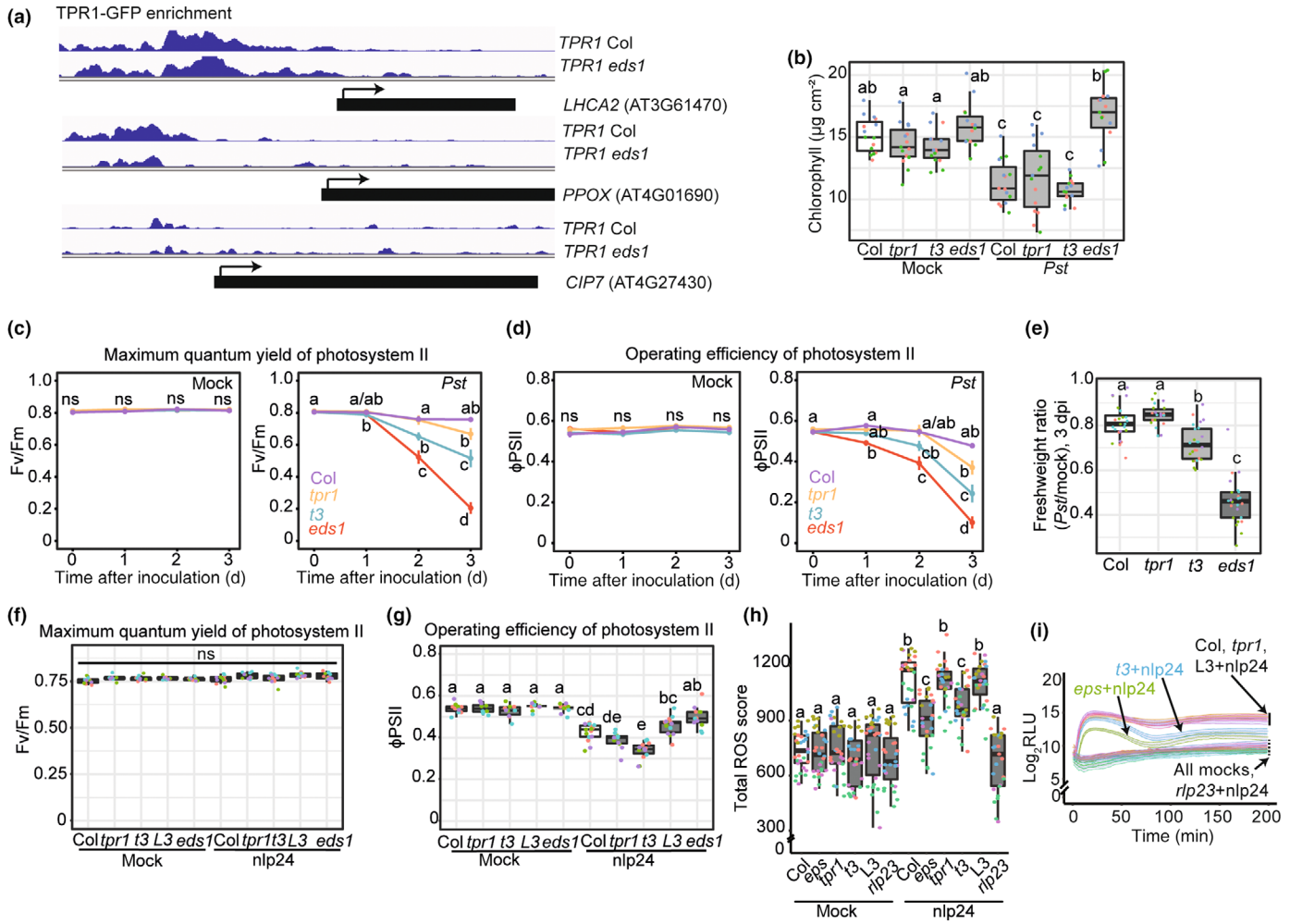

Fig. 5 TPR1 limits adverse effects of nlp24-activated PTI on *Arabidopsis* PSII performance. (a) Genes with chloroplast functions are direct binding targets of TPR1. Input-normalized ChIP-Seq profiles show that TPR1-GFP binds in *TPR1* Col and *TPR1 eds1* at the upstream sequences of *LHCA2* (AT3G61470), *PPOX* (AT4G01690), and *CIP7* (AT4G27430) involved in photosynthesis or chlorophyll biosynthesis. (b) *tpr1* and *t3* mutants display the Col-like chlorophyll reduction after *Pst* infection. Plants of indicated genotypes were syringe-infiltrated with *Pst* ($OD_{600} = 0.005$) and total (*a* + *b*) chlorophyll content was determined at 3d post-inoculation (dpi) (Tukey's HSD $\alpha = 0.05$; $n = 15$ from three independent experiments). (c, d) Maximum quantum yield of PSII (F_v/F_m) (c) and operating PSII efficiency (φPSII) (d) in indicated genotypes over the 3-d time course after syringe infiltration of *Pst* ($OD_{600} = 0.005$; left panels). Compared with Col, the *t3* mutant shows significantly reduced F_v/F_m at 3 d after infection with *Pst* but not in the mock-treated samples (Tukey's HSD $\alpha = 0.05$; $n = 9$–12 from three independent experiments). Error bars represent SEM. (e) Fresh weight reduction in leaves inoculated with *Pst* ($OD_{600} = 0.005$) compared with mock-treated leaves in indicated genotypes 3 dpi (Tukey's HSD $\alpha = 0.05$; $n = 20$–24 from four independent experiments). (f, g) F_v/F_m (f) and φPSII (g) in indicated genotypes 3 dpi after syringe infiltration of 5 µM nlp24 or mock (10 mM $MgCl_2$) control (Tukey's HSD $\alpha = 0.05$; $n = 10$–14 from four independent experiments). φPSII drops stronger in the *t3* mutant but this is restored to Col levels in the complementation line L3 (*pTPR1:TPR1-GFP* L3; *t3* background). (h, i) Reactive oxygen species burst in the indicated genotypes in the presence of nlp24 (2 µM). (h) Total ROS score is a sum of log_2-transformed relative luminescence units (RLU) recorded over the time course 200 min. ROS burst is lower in the *t3* and *eds1-12 pad4-1 sag101-3* (*eps*) mutant compared with Col and the L3 complementation line. (i) The difference between Col and *t3* (blue ribbon) is visible after *c*. 1 h after exposure to nlp24 (Tukey's HSD $\alpha = 0.05$; $n = 27$–30 from five independent experiments). Shadowing around lines corresponds to one SEM. ns, not significant. Elements of boxplots and matching population statistics: first quartile – minima, third quartile – maxima, median – central line; whiskers extend to the minimum and maximum values but not further than 1.5 interquartile range from the respective minima or maxima of the boxplot. Datapoints with the same color were recorded in one independent experiment. Non-overlapping lowercase letter combinations in (b–e, g–i) indicate that the samples have statistically significant differences (Tukey's HSD $\alpha = 0.05$).

Our RNA-Seq gene expression data do not support the role of TPR1 and other TPL/TPRs in *EDS1*-dependent transcriptional host defense mobilization at 8 or 24 h after bacterial inoculation despite compromised resistance of the *t3* mutant to different *Pst* strains (Fig. 3a–d). How then do TPL/TPRs positively regulate *Arabidopsis* defense against bacteria? An earlier report showed that TPR1 and other TPL/TPRs contribute to PAMP-triggered ROS burst from the surface receptor FLS2 (Navarrete *et al.*, 2021) that is largely *EDS1*-independent (Pruitt *et al.*, 2021; Tian *et al.*, 2021). We find that nlp24-triggered RLP23 and EDS1 family-dependent ROS burst is reduced in the *t3* mutant but it recovered in the complementation lines

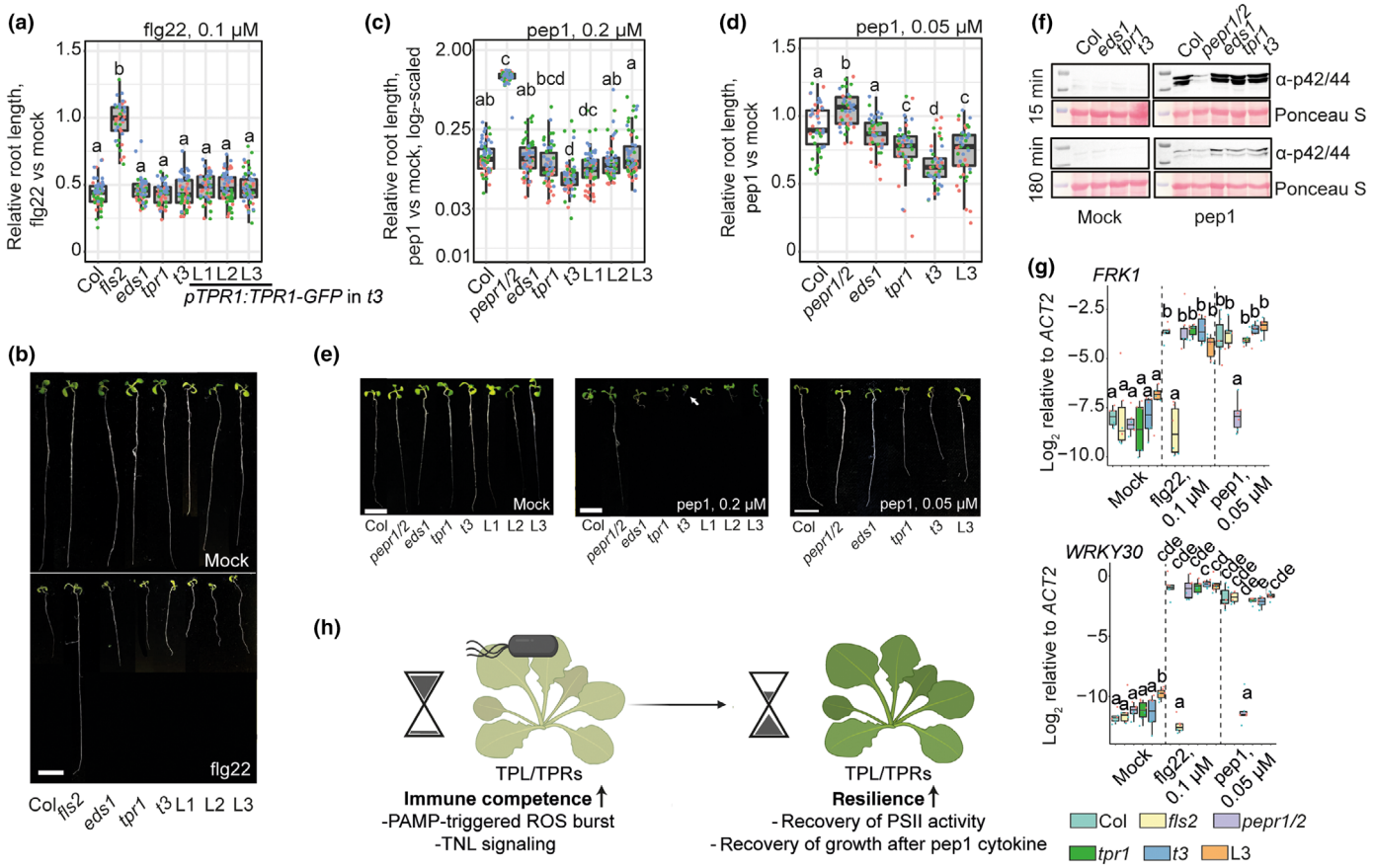

Fig. 6 TPR1 limits phytocytokine pep1 inhibition of *Arabidopsis* growth. (a) Inhibition of the main root growth in 10-d-old seedlings of indicated genotypes grown on liquid 0.5× MS supplemented with flg22 (100 nM). The *eds1*, *tpr1*, *t3* mutants as well as the *pTPR1:TPR1-GFP* complementation lines (L1–L3) showed the Col-like root growth inhibition, while the flg22 receptor mutant *fls2* was insensitive to the treatment (Tukey's HSD $\alpha = 0.05$; $n = 58$ from three independent experiments). The main root length in flg22-treated plants was normalized to the respective mean in mock-treated seedlings. (b) Photographs of representative seedlings measured in (a). Bar, 1 cm. (c, d) Boxplot representation of root growth ratio after exposure of 10-d-old seedlings of indicated genotypes on 0.5× liquid MS medium with 0.2 μM (c) or 0.05 μM (d) pep1 relative to the mock (mQ water) treatment (Tukey's HSD $\alpha = 0.05$; $n = 58$ and $n = 48$ from three independent experiments in c and d, respectively). *Y*-axis in (c) is $\log_2$-scaled. The *t3* mutant is hypersensitive to pep1 at the level of root growth inhibition, but this is recovered in the L3 complementation line. (e) Representative photographs of seedlings from (c) and (d). Bar, 1 cm. (f) MPK3 and MPK6 phosphorylation assessed via Western blot analysis with α-p42/44 antibodies in indicated genotypes at 15 and 180 min after mock (mQ water) or pep1 (0.2 μM) treatment. The *t3* mutant showed Col level of MPK3 and MPK6 phosphorylation. The experiment was repeated three times with similar results. In (a–f), *eds1* is *eds1-12*. (g) Induction of PTI marker genes *FRK1* (FLG22-induced receptor-like kinase 1) and *WRKY30* in seedlings of indicated genotypes after exposure to flg22 (0.1 μM), pep1 (0.05 μM) or mock (mQ) for 1 h. Seedlings were grown on liquid 0.5× MS for 11 d (red datapoints) or 12 d (blue datapoints). The *tpr1*, *t3* mutants and the complementation line L3 responded similarly (Tukey's HSD $\alpha = 0.05$; $n = 6$ from two independent experiments). (h) Model of the function of TPR1 and other TPL/TPRs in immune-triggered Arabidopsis leaves. TPL/TPRs promote immune activation in the initial response (e.g. ROS production) but help to maintain PSII activity and growth at later stages of the immune responses. The picture was created with BioRender.com. Elements of boxplots and matching population statistics: first quartile – minima, third quartile – maxima, median –central line; whiskers extend to the minimum and maximum values but not further than 1.5 interquartile range from the respective minima or maxima of the boxplot. Datapoints with the same color were recorded in one independent experiment. Non-overlapping letter combinations above the boxplots in (a, c, d, g) show statistically significant differences between the samples (Tukey's HSD $\alpha = 0.05$).

(Fig. 5h,i). Thus, TPR1 and probably other TPL/TPRs contribute to a PTI-associated ROS burst. This defect in PTI might explain weakly reduced expression of gene sets from GO terms linked to immunity in *tpr1* and *t3* mutants after *Pst avrRps4* infiltration (Fig. 3e; *c.* 5 min). Although TPR1 contributes to TNL snc1 signaling (Zhu *et al.*, 2010; Zhang *et al.*, 2019; Navarrete *et al.*, 2021), which in turn requires the EDS1 family, it is still unclear whether a TPL/TPRs contribution to PAMP ROS burst occurs via TIR domain signaling. In addition, TPR1 was proposed to induce defenses by repressing negative regulators of resistance (Zhu *et al.*, 2010). Consistent with this view, TPR1 is enriched at promoters of genes that are repressed during $TNL^{RRS1\text{-}RPS4}$ ETI (Fig. S3; Bartsch *et al.*, 2006; Zhu *et al.*, 2010), and TPR1 can repress *DND1/CNGC2* and *DND2/CNGC4* promoter activity (Niu *et al.*, 2019).

The *t3* mutant over-responded at the level of defense-associated gene expression at 24 hpi with *Pst avrRps4* bacteria and bacteria-triggered electrolyte leakage (Fig. 3). Also, we identified a contribution of TPR1 and other TPL/TPRs to supporting photosystem II activity in leaves infected with *Pst* or infiltrated

with PAMP nlp24 and in maintaining seedling growth in response to pep1 (Figs 5, 6). Hence, a model emerges in which *Arabidopsis* TPR1 and other TPL/TPRs transcriptional corepressors promote initial immune activation (Figs 3e, 5i) but subsequently mitigate adverse effects of activated immunity signaling on host physiology and growth (Fig. 6h). Interestingly, TPR2 and TPR3 likely work as negative regulators of TNL snc1-conditioned autoimmunity and shoot growth retardation (Garner *et al.*, 2021). Thus, both clades of the TPL/TPR family, TPR1/TPL/TPR4 and TPR2/TPR3, can help to reduce damaging effects of activated immunity in *Arabidopsis*.

Timely downregulation of defense signaling is relevant because prolonged pathogen infection and plant immune activation often lead to reduced photosynthetic activity and biomass (Walters, 2015a,b). Pathogen-free induction of SA and JA signaling is associated with reduced expression of genes involved in photosynthesis (Hickman *et al.*, 2017, 2019). Despite the identification of multiple genes affecting the balance of growth and defense (Huot *et al.*, 2014; Bruessow *et al.*, 2021), knowledge of how plants turn down transcriptional defenses and regain physiological homeostasis is fragmentary. Cytoplasmic condensates of the SA receptor NPR1 were reported to be responsible for the ubiquitination of ETI cell death-promoting WRKY TFs to limit their activities (Zavaliev *et al.*, 2020). Also, the SA receptor NPR4 suppresses *Arabidopsis* WRKY70 promoter activity (Ding *et al.*, 2018). Our study identifies *Arabidopsis* transcriptional corepressor TPR1 as a factor that prevents overshooting of an immune response and therefore as a potential contributor to plant stress-fitness balance.

Acknowledgements

This work was supported by the Max-Planck Society and Deutsche Forschungsgemeinschaft (DFG) (grants SFB-1403–414786233 and CRC-670 TP19 to JEP; DL), and the FU Berlin (TG). We thank Yuelin Zhang for providing *pTPR1:TPR1-GFP*, *pTPR1:TPR1-HA*, *tpr1*, *t3* lines, and *pCAMBIA1305-TPR1-GFP* vector, Johannes Stuttmann for *eds1-12*, and Rainer Birkenbihl for advice on ChIP methodology. We thank the Max Planck-Genome-center Cologne for sequencing of ChIP- and RNA samples in this study (http://mpgc.mpipz.mpg.de/home/). We also thank Guido van den Ackerveken (Utrecht University) for helpful discussions and for providing resources for the experimental work. Open Access funding enabled and organized by Projekt DEAL.

Competing interests

None declared.

Author contributions

TG, DL, FL, and JEP designed experiments. TG, DL, and FL performed experiments. TG, DL, and JEP analyzed all data. BK, LC, and MB analyzed ChIP-Seq and RNA-Seq. JB and DL generated and characterized complementation lines. DL prepared the Github repository and materials for access to processed ChIP-Seq data. TG, DL, and JEP wrote the manuscript with input from all authors. TG and DL contributed equally to this work.

ORCID

Moussa Benhamed https://orcid.org/0000-0002-2716-748X
Lorenzo Concia https://orcid.org/0000-0002-7401-7214
Thomas Griebel https://orcid.org/0000-0002-3600-6493
Dmitry Lapin https://orcid.org/0000-0001-9591-3950
Federica Locci https://orcid.org/0000-0001-5443-0717
Jane E. Parker https://orcid.org/0000-0002-4700-6480

Data availability

RNA-Seq and ChIP-Seq data from this article are deposited in the National Center for Biotechnology Information Gene Expression Omnibus (GEO) database with accession nos. GSE149316, GSE154652, and GSE154774. Bigwig, BAM, and BAI files of TPR1 ChIP-Seq for visualization in IGV browser are also available through the Max Planck Digital Library collection (MPDL; https://edmond.mpdl.mpg.de/imeji/collection/U6N5zIOIWgjjMZCu). Scripts for preparing metaplots in R environment on a personal computer (*c.* 8G RAM) are on GitHub (https://github.com/rittersporn/TPR1_metaplots_Griebel_Lapin_etal_2021).

References

Albert I, Bohm H, Albert M, Feiler CE, Imkampe J, Wallmeroth N, Brancato C, Raaymakers TM, Oome S, Zhang H *et al.* 2015. An RLP23-SOBIR1-BAK1 complex mediates NLP-triggered immunity. *Nature Plants* **1**: 15140.

Albert I, Hua C, Nürnberger T, Pruitt RN, Zhang L. 2020. Surface sensor systems in plant immunity. *Plant Physiology* **182**: 1582–1596.

Ariga H, Katori T, Tsuchimatsu T, Hirase T, Tajima Y, Parker JE, Alcázar R, Koornneef M, Hoekenga O, Lipka AE *et al.* 2017. NLR locus-mediated trade-off between abiotic and biotic stress adaptation in Arabidopsis. *Nature Plants* **3**: 17072.

Baker NR. 2008. Chlorophyll fluorescence: a probe of photosynthesis *in vivo*. *Annual Review of Plant Biology* **59**: 89–113.

Bartsch M, Gobbato E, Bednarek P, Debey S, Schultze JL, Bautor J, Parker JE. 2006. Salicylic acid-independent ENHANCED DISEASE SUSCEPTIBILITY1 signaling in Arabidopsis immunity and cell death is regulated by the monooxygenase FMO1 and the Nudix hydrolase NUDT7. *Plant Cell* **18**: 1038–1051.

Bhandari DD, Lapin D, Kracher B, von Born P, Bautor J, Niefind K, Parker JE. 2019. An EDS1 heterodimer signalling surface enforces timely reprogramming of immunity genes in Arabidopsis. *Nature Communications* **10**: 772.

Birkenbihl RP, Kracher B, Roccaro M, Somssich IE. 2017. Induced genome-wide binding of three Arabidopsis WRKY transcription factors during early MAMP-triggered immunity. *Plant Cell* **29**: 20–38.

Birkenbihl RP, Kracher B, Ross A, Kramer K, Finkemeier I, Somssich IE. 2018. Principles and characteristics of the Arabidopsis WRKY regulatory network during early MAMP-triggered immunity. *The Plant Journal* **96**: 487–502.

Bruessow F, Bautor J, Hoffmann G, Yildiz I, Zeier J, Parker JE. 2021. Natural variation in temperature-modulated immunity uncovers transcription factor bHLH059 as a thermoresponsive regulator in *Arabidopsis thaliana*. *PLoS Genetics* **17**: e1009290.

van Butselaar T, Van den Ackerveken G. 2020. Salicylic acid steers the growth–immunity tradeoff. *Trends in Plant Science* **25**: 566–576.

Caarls L, Elberse J, Awwanah M, Ludwig NR, de Vries M, Zeilmaker T, Van Wees SCM, Schuurink RC, Van den Ackerveken G. 2017. *Arabidopsis* JASMONATE-INDUCED OXYGENASES down-regulate plant immunity by hydroxylation and inactivation of the hormone jasmonic acid. *Proceedings of the National Academy of Sciences, USA* **114**: 6388–6393.

Causier B, Ashworth M, Guo W, Davies B. 2012. The TOPLESS interactome: a framework for gene repression in Arabidopsis. *Plant Physiology* **158**: 423–438.

Ciolkowski I, Wanke D, Birkenbihl RP, Somssich IE. 2008. Studies on DNA-binding selectivity of WRKY transcription factors lend structural clues into WRKY-domain function. *Plant Molecular Biology* **68**: 81–92.

Clough SJ, Fengler KA, Yu IC, Lippok B, Smith RK, Bent AF. 2000. The *Arabidopsis dnd1* "defense, no death" gene encodes a mutated cyclic nucleotide-gated ion channel. *Proceedings of the National Academy of Sciences, USA* **97**: 9323–9328.

Copeland C, Li X. 2019. Chapter 2 – Regulation of plant immunity by the proteasome. In: Galluzzi L, ed. *International review of cell and molecular biology*. New York, NY, USA: Academic Press, Weill Cornell Medical College, 37–63.

Cui H, Qiu J, Zhou Y, Bhandari DD, Zhao C, Bautor J, Parker JE. 2018. Antagonism of transcription factor MYC2 by EDS1/PAD4 complexes bolsters salicylic acid defense in Arabidopsis effector-triggered immunity. *Molecular Plant* **11**: 1053–1066.

Cui H, Tsuda K, Parker JE. 2015. Effector-triggered immunity: from pathogen perception to robust defense. *Annual Review of Plant Biology* **66**: 487–511.

Darino M, Chia K-S, Marques J, Aleksza D, Soto-Jiménez LM, Saado I, Uhse S, Borg M, Betz R, Bindics J *et al.* 2021. *Ustilago maydis* effector Jsi1 interacts with Topless corepressor, hijacking plant jasmonate/ethylene signaling. *New Phytologist* **229**: 3393–3407.

Deng Y, Zhai K, Xie Z, Yang D, Zhu X, Liu J, Wang X, Qin P, Yang Y, Zhang G *et al.* 2017. Epigenetic regulation of antagonistic receptors confers rice blast resistance with yield balance. *Science* **355**: 962–965.

Ding P, Ngou BPM, Furzer OJ, Sakai T, Shrestha RK, MacLean D, Jones JDG. 2020. High-resolution expression profiling of selected gene sets during plant immune activation. *Plant Biotechnology Journal* **18**: 1610–1619.

Ding Y, Sun T, Ao K, Peng Y, Zhang Y, Li X, Zhang Y. 2018. Opposite roles of salicylic acid receptors NPR1 and NPR3/NPR4 in transcriptional regulation of plant immunity. *Cell* **173**: 1454–1467.

Dongus JA, Parker JE. 2021. EDS1 signalling: at the nexus of intracellular and surface receptor immunity. *Current Opinion in Plant Biology* **62**: 102039.

Dowen RH, Pelizzola M, Schmitz RJ, Lister R, Dowen JM, Nery JR, Dixon JE, Ecker JR. 2012. Widespread dynamic DNA methylation in response to biotic stress. *Proceedings of the National Academy of Sciences, USA* **109**: E2183–E2191.

Dvořák Tomaštíková E, Hafrén A, Trejo-Arellano MS, Rasmussen SR, Sato H, Santos-González J, Köhler C, Hennig L, Hofius D. 2021. Polycomb repressive complex 2 and KRYPTONITE regulate pathogen-induced programmed cell death in Arabidopsis. *Plant Physiology* **185**: 2003–2021.

Fradin EF, Abd-El-Haliem A, Masini L, van den Berg GC, Joosten MH, Thomma BP. 2011. Interfamily transfer of tomato Ve1 mediates *Verticillium* resistance in Arabidopsis. *Plant Physiology* **156**: 2255–2265.

Garner CM, Spears BJ, Su J, Cseke LJ, Smith SN, Rogan CJ, Gassmann W. 2021. Opposing functions of the plant TOPLESS gene family during SNC1-mediated autoimmunity. *PLoS Genetics* **17**: e1009026.

Goralogia GS, Liu T-K, Zhao L, Panipinto PM, Groover ED, Bains YS, Imaizumi T. 2017. CYCLING DOF FACTOR 1 represses transcription through the TOPLESS co-repressor to control photoperiodic flowering in Arabidopsis. *The Plant Journal* **92**: 244–262.

Gorham SR, Weiner AI, Yamadi M, Krogan NT. 2018. HISTONE DEACETYLASE 19 and the flowering time gene FD maintain reproductive meristem identity in an age-dependent manner. *Journal of Experimental Botany* **69**: 4757–4771.

Harvey S, Kumari P, Lapin D, Griebel T, Hickman R, Guo W, Zhang R, Parker JE, Beynon J, Denby K *et al.* 2020. Downy mildew effector HaRxL21 interacts with the transcriptional repressor TOPLESS to promote pathogen susceptibility. *PLoS Pathogens* **16**: e1008835.

Heidrich K, Wirthmueller L, Tasset C, Pouzet C, Deslandes L, Parker JE. 2011. *Arabidopsis* EDS1 connects pathogen effector recognition to cell compartment–specific immune responses. *Science* **334**: 1401–1404.

Hickman R, Mendes MP, Van Verk MC, Van Dijken AJH, Di Sora J, Denby K, Pieterse CMJ, Van Wees SCM. 2019. Transcriptional dynamics of the salicylic acid response and its interplay with the jasmonic acid pathway. *bioRxiv*. doi: 10.1101/742742.

Hickman R, Van Verk MC, Van Dijken AJH, Mendes MP, Vroegop-Vos IA, Caarls L, Steenbergen M, Van der Nagel I, Wesselink GJ, Jironkin A *et al.* 2017. Architecture and dynamics of the jasmonic acid gene regulatory network. *Plant Cell* **29**: 2086–2105.

Huang C-Y, Rangel DS, Qin X, Bui C, Li R, Jia Z, Cui X, Jin H. 2021. The chromatin-remodeling protein BAF60/SWP73A regulates the plant immune receptor NLRs. *Cell Host & Microbe* **29**: 425–434.

Huot B, Yao J, Montgomery BL, He SY. 2014. Growth–defense tradeoffs in plants: a balancing act to optimize fitness. *Molecular Plant* **7**: 1267–1287.

Igarashi D, Tsuda K, Katagiri F. 2012. The peptide growth factor, phytosulfokine, attenuates pattern-triggered immunity. *The Plant Journal* **71**: 194–204.

Jones JDG, Vance RE, Dangl JL. 2016. Intracellular innate immune surveillance devices in plants and animals. *Science* **354**: aaf6395.

Jurkowski GI, Smith RK, Yu I, Ham JH, Sharma SB, Klessig DF, Fengler KA, Bent AF. 2004. Arabidopsis DND2, a second cyclic nucleotide-gated ion channel gene for which mutation causes the "defense, no death" phenotype. *Molecular Plant–Microbe Interactions* **17**: 511–520.

Ke J, Ma H, Gu X, Thelen A, Brunzelle JS, Li J, Xu HE, Melcher K. 2015. Structural basis for recognition of diverse transcriptional repressors by the TOPLESS family of corepressors. *Science Advances* **1**: e1500107.

Krol E, Mentzel T, Chinchilla D, Boller T, Felix G, Kemmerling B, Postel S, Arents M, Jeworutzki E, Al-Rasheid KAS *et al.* 2010. Perception of the *Arabidopsis* danger signal peptide 1 involves the pattern recognition receptor *At*PEPR1 and its close homologue *At*PEPR2. *Journal of Biological Chemistry* **285**: 13471–13479.

Kuhn A, Ramans Harborough S, McLaughlin HM, Natarajan B, Verstraeten I, Friml J, Kepinski S, Østergaard L. 2020. Direct ETTIN-auxin interaction controls chromatin states in gynoecium development. *eLife* **9**: e51787.

Lapin D, Bhandari DD, Parker JE. 2020. Origins and immunity networking functions of EDS1 family proteins. *Annual Review of Phytopathology* **58**: 253–276.

Lapin D, Kovacova V, Sun X, Dongus JA, Bhandari D, von Born P, Bautor J, Guarneri N, Rzemieniewski J, Stuttmann J *et al.* 2019. A coevolved EDS1-SAG101-NRG1 module mediates cell death signaling by TIR-domain immune receptors. *Plant Cell* **31**: 2430–2455.

Lee HG, Won JH, Choi Y-R, Lee K, Seo PJ. 2020. Brassinosteroids regulate circadian oscillation via the BES1/TPL-CCA1/LHY module in *Arabidopsis thaliana*. *iScience* **23**: 101528.

Leng X, Thomas Q, Rasmussen SH, Marquardt S. 2020. A G(enomic)P(ositioning)S(ystem) for plant RNAPII transcription. *Trends in Plant Science* **25**: 744–764.

Leydon AR, Wang W, Gala HP, Gilmour S, Juarez-Solis S, Zahler ML, Zemke JE, Zheng N, Nemhauser JL. 2021. Repression by the Arabidopsis TOPLESS corepressor requires association with the core mediator complex. *bioRxiv*. doi: 10.1101/2020.03.04.976134.

Long JA, Ohno C, Smith ZR, Meyerowitz EM. 2006. TOPLESS regulates apical embryonic fate in *Arabidopsis*. *Science* **312**: 1520–1523.

Lorenzo O, Chico JM, Sánchez-Serrano JJ, Solano R. 2004. JASMONATE-INSENSITIVE1 encodes a MYC transcription factor essential to discriminate between different jasmonate-regulated defense responses in Arabidopsis. *Plant Cell* **16**: 1938–1950.

Ma H, Duan J, Ke J, He Y, Gu X, Xu T-H, Yu H, Wang Y, Brunzelle JS, Jiang Y *et al.* 2017. A D53 repression motif induces oligomerization of TOPLESS corepressors and promotes assembly of a corepressor-nucleosome complex. *Science Advances* **3**: e1601217.

Martin-Arevalillo R, Nanao MH, Larrieu A, Vinos-Poyo T, Mast D, Galvan-Ampudia C, Brunoud G, Vernoux T, Dumas R, Parcy F. 2017. Structure of the *Arabidopsis* TOPLESS corepressor provides insight into the evolution of transcriptional repression. *Proceedings of the National Academy of Sciences, USA* **114**: 8107–8112.

Mine A, Seyfferth C, Kracher B, Berens ML, Becker D, Tsuda K. 2018. The defense phytohormone signaling network enables rapid, high-amplitude

transcriptional reprogramming during effector-triggered immunity. *Plant Cell* **30**: 1199–1219.

Navarrete F, Gallei M, Kornienko AE, Saado I, Khan M, Chia K-S, Darino MA, Bindics J, Djamei A. 2021. TOPLESS promotes plant immunity by repressing auxin signaling and is targeted by the fungal effector Naked1. *Plant Communications* **3**: 100269.

Ngou BPM, Ahn H-K, Ding P, Jones JDG. 2021. Mutual potentiation of plant immunity by cell-surface and intracellular receptors. *Nature* **592**: 110–115.

Niu D, Lin X-L, Kong X, Qu G-P, Cai B, Lee J, Jin JB. 2019. SIZ1-mediated SUMOylation of TPR1 suppresses plant immunity in Arabidopsis. *Molecular Plant* **12**: 215–228.

Oome S, Raaymakers TM, Cabral A, Samwel S, Bohm H, Albert I, Nurnberger T, Van den Ackerveken G. 2014. Nep1-like proteins from three kingdoms of life act as a microbe-associated molecular pattern in Arabidopsis. *Proceedings of the National Academy of Sciences, USA* **111**: 16955–16960.

Ordon J, Gantner J, Kemna J, Schwalgun L, Reschke M, Streubel J, Boch J, Stuttmann J. 2017. Generation of chromosomal deletions in dicotyledonous plants employing a user-friendly genome editing toolkit. *The Plant Journal* **89**: 155–168.

Pauwels L, Barbero GF, Geerinck J, Tilleman S, Grunewald W, Pérez AC, Chico JM, Bossche RV, Sewell J, Gil E *et al.* 2010. NINJA connects the co-repressor TOPLESS to jasmonate signalling. *Nature* **464**: 788–791.

Plant AR, Larrieu A, Causier B. 2021. Repressor for hire! The vital roles of TOPLESS-mediated transcriptional repression in plants. *New Phytologist* **231**: 963–973.

Porra RJ, Thompson WA, Kriedemann PE. 1989. Determination of accurate extinction coefficients and simultaneous-equations for assaying chlorophyll-a and chlorophyll-b extracted with four different solvents - verification of the concentration of chlorophyll standards by atomic absorption spectroscopy. *Biochimica et Biophysica Acta* **975**: 384–394.

Pruitt RN, Locci F, Wanke F, Zhang L, Saile SC, Joe A, Karelina D, Hua C, Frohlich K, Wan WL *et al.* 2021. The EDS1-PAD4-ADR1 node mediates Arabidopsis pattern-triggered immunity. *Nature* **598**: 495–499.

Qiao Y, Xia R, Zhai J, Hou Y, Feng L, Zhai Y, Ma W. 2021. Small RNAs in plant immunity and virulence of filamentous pathogens. *Annual Review of Phytopathology* **59**: 265–288.

Saile SC, Jacob P, Castel B, Jubic LM, Salas-Gonzáles I, Bäcker M, Jones JDG, Dangl JL, El Kasmi F. 2020. Two unequally redundant "helper" immune receptor families mediate *Arabidopsis thaliana* intracellular "sensor" immune receptor functions. *PLoS Biology* **18**: e3000783.

Saucet SB, Ma Y, Sarris PF, Furzer OJ, Sohn KH, Jones JDG. 2015. Two linked pairs of Arabidopsis TNL resistance genes independently confer recognition of bacterial effector AvrRps4. *Nature Communications* **6**: 6338.

Seidl MF, Van den Ackerveken G. 2019. Activity and phylogenetics of the broadly occurring family of microbial Nep1-like proteins. *Annual Review of Phytopathology* **57**: 367–386.

Shen L, Shao N-Y, Liu X, Maze I, Feng J, Nestler EJ. 2013. diffReps: detecting differential chromatin modification sites from ChIP-seq data with biological replicates. *PLoS ONE* **8**: e65598.

Sohn KH, Segonzac C, Rallapalli G, Sarris PF, Woo JY, Williams SJ, Newman TE, Paek KH, Kobe B, Jones JDG. 2014. The nuclear immune receptor RPS4 is required for RRS1SLH1-dependent constitutive defense activation in *Arabidopsis thaliana*. *PLoS Genetics* **10**: e1004655.

Straus MR, Rietz S, Loren V, van Themaat E, Bartsch M, Parker JE. 2010. Salicylic acid antagonism of EDS1-driven cell death is important for immune and oxidative stress responses in Arabidopsis. *The Plant Journal* **62**: 628–640.

Sun T, Zhang Y, Li Y, Zhang Q, Ding Y, Zhang Y. 2015. ChIP-seq reveals broad roles of SARD1 and CBP60g in regulating plant immunity. *Nature Communications* **6**: 10159.

Sun X, Lapin D, Feehan JM, Stolze SC, Kramer K, Dongus JA, Rzemieniewski J, Blanvillain-Baufumé S, Harzen A, Bautor J *et al.* 2021. Pathogen effector recognition-dependent association of NRG1 with EDS1 and SAG101 in TNL receptor immunity. *Nature Communications* **12**: 3335.

Szemenyei H, Hannon M, Long JA. 2008. TOPLESS mediates auxin-dependent transcriptional repression during *Arabidopsis* embryogenesis. *Science* **319**: 1384–1386.

Tian H, Wu Z, Chen S, Ao K, Huang W, Yaghmaiean H, Sun T, Xu F, Zhang Y, Wang S *et al.* 2021. Activation of TIR signalling boosts pattern-triggered immunity. *Nature* **598**: 500–503.

Tian W, Hou C, Ren Z, Wang C, Zhao F, Dahlbeck D, Hu S, Zhang L, Niu Q, Li L *et al.* 2019. A calmodulin-gated calcium channel links pathogen patterns to plant immunity. *Nature* **572**: 131–135.

Todesco M, Balasubramanian S, Hu TT, Traw MB, Horton M, Epple P, Kuhns C, Sureshkumar S, Schwartz C, Lanz C *et al.* 2010. Natural allelic variation underlying a major fitness trade-off in *Arabidopsis thaliana*. *Nature* **465**: 632–636.

Tsuda K, Somssich IE. 2015. Transcriptional networks in plant immunity. *New Phytologist* **206**: 932–947.

Van Moerkercke A, Duncan O, Zander M, Šimura J, Broda M, Vanden Bossche R, Lewsey MG, Lama S, Singh KB, Ljung K *et al.* 2019. A MYC2/MYC3/MYC4-dependent transcription factor network regulates water spray-responsive gene expression and jasmonate levels. *Proceedings of the National Academy of Sciences, USA* **116**: 23345–23356.

Wagner S, Stuttmann J, Rietz S, Guerois R, Brunstein E, Bautor J, Niefind K, Parker JE. 2013. Structural basis for signaling by exclusive EDS1 heteromeric complexes with SAG101 or PAD4 in plant innate immunity. *Cell Host & Microbe* **14**: 619–630.

Walters DR. 2015a. Growth, development and yield of infected and infested plants and crops. In: *Physiological responses of plants to attack*. Chichester, UK: John Wiley & Sons, 24–40.

Walters DR. 2015b. Photosynthesis in attacked plants and crops. In: *Physiological responses of plants to attack*. Chichester, UK: John Wiley & Sons, 41–87.

Wang H, Li S, Li Y, Xu Y, Wang Y, Zhang R, Sun W, Chen Q, Wang X-J, Li C *et al.* 2019. MED25 connects enhancer–promoter looping and MYC2-dependent activation of jasmonate signalling. *Nature Plants* **5**: 616–625.

Wildermuth MC, Dewdney J, Wu G, Ausubel FM. 2001. Isochorismate synthase is required to synthesize salicylic acid for plant defence. *Nature* **414**: 562–565.

Yang L, Teixeira PJPL, Biswas S, Finkel OM, He Y, Salas-Gonzalez I, English ME, Epple P, Mieczkowski P, Dangl JL. 2017. *Pseudomonas syringae* type III effector HopBB1 promotes host transcriptional repressor degradation to regulate phytohormone responses and virulence. *Cell Host & Microbe* **21**: 156–168.

Yu A, Lepère G, Jay F, Wang J, Bapaume L, Wang Y, Abraham A-L, Penterman J, Fischer RL, Voinnet O *et al.* 2013. Dynamics and biological relevance of DNA demethylation in *Arabidopsis* antibacterial defense. *Proceedings of the National Academy of Sciences, USA* **110**: 2389–2394.

Yu C-P, Lin J-J, Li W-H. 2016. Positional distribution of transcription factor binding sites in *Arabidopsis thaliana*. *Scientific Reports* **6**: 25164.

Yuan M, Jiang Z, Bi G, Nomura K, Liu M, Wang Y, Cai B, Zhou J-M, He SY, Xin X-F. 2021. Pattern-recognition receptors are required for NLR-mediated plant immunity. *Nature* **592**: 105–109.

Zander M, Lewsey MG, Clark NM, Yin L, Bartlett A, Saldierna Guzmán JP, Hann E, Langford AE, Jow B, Wise A *et al.* 2020. Integrated multi-omics framework of the plant response to jasmonic acid. *Nature Plants* **6**: 290–302.

Zavaliev R, Mohan R, Chen T, Dong X. 2020. Formation of NPR1 condensates promotes cell survival during the plant immune response. *Cell* **182**: 1093–1108.

Zervudacki J, Yu A, Amesefe D, Wang J, Drouaud J, Navarro L, Deleris A. 2018. Transcriptional control and exploitation of an immune-responsive family of plant retrotransposons. *EMBO Journal* **37**: e98482.

Zhang Y, Goritschnig S, Dong X, Li X. 2003. A gain-of-function mutation in a plant disease resistance gene leads to constitutive activation of downstream signal transduction pathways in suppressor of npr1-1, constitutive 1. *Plant Cell* **15**: 2636–2646.

Zhang Y, Song G, Lal NK, Nagalakshmi U, Li Y, Zheng W, Huang P-J, Branon TC, Ting AY, Walley JW *et al.* 2019. TurboID-based proximity labeling reveals that UBR7 is a regulator of N NLR immune receptor-mediated immunity. *Nature Communications* **10**: 3252.

Zhang Y, Xu S, Ding P, Wang D, Cheng YT, He J, Gao M, Xu F, Li Y, Zhu Z *et al.* 2010. Control of salicylic acid synthesis and systemic acquired resistance by two members of a plant-specific family of transcription factors. *Proceedings of the National Academy of Sciences, USA* **107**: 18220–18225.

Zheng X-Y, Spivey Natalie W, Zeng W, Liu P-P, Fu Zheng Q, Klessig Daniel F, He Sheng Y, Dong X. 2012. Coronatine promotes *Pseudomonas syringae* virulence in plants by activating a signaling cascade that inhibits salicylic acid accumulation. *Cell Host & Microbe* **11**: 587–596.

Zhou M, Lu Y, Bethke G, Harrison BT, Hatsugai N, Katagiri F, Glazebrook J. 2018. WRKY70 prevents axenic activation of plant immunity by direct repression of SARD1. *New Phytologist* **217**: 700–712.

Zhu Z, Xu F, Zhang Y, Cheng YT, Wiermer M, Li X, Zhang Y. 2010. Arabidopsis resistance protein SNC1 activates immune responses through association with a transcriptional corepressor. *Proceedings of the National Academy of Sciences, USA* **107**: 13960–13965.

Zipfel C, Robatzek S, Navarro L, Oakeley EJ, Jones JDG, Felix G, Boller T. 2004. Bacterial disease resistance in Arabidopsis through flagellin perception. *Nature* **428**: 764–767.

Supporting Information

Additional Supporting Information may be found online in the Supporting Information section at the end of the article.

Fig. S1 Autoimmunity of *TPR1* Col is *EDS1*-dependent.

Fig. S2 Input-normalized ChIP-Seq profiles of TPR1-GFP in *TPR1* Col and *TPR1 eds1* at selected genes showing differential TPR1-GFP binding and expression in *TPR1* Col and *TPR1 eds1*.

Fig. S3 Input-normalized ChIP-Seq profiles of TPR1-GFP in *TPR1* Col and *TPR1 eds1* at the indicated genes bound by hemagglutinin tagged TPR1 in autoimmune *TPR1-HA* Col line in Zhu *et al.* (2010).

Fig. S4 Input-normalized ChIP-Seq profiles of TPR1-GFP in *TPR1* Col and *TPR1 eds1* at genes known as targets of TPL.

Fig. S5 MYC, WRKYs, and SARD1 chromatin binding events are enriched at the TPR1-bound loci.

Fig. S6 The *tpr1 tpl tpr4* mutant showed enhanced defense transcriptional reprogramming at 24 hpi with *Pst avrRps4*.

Methods S1 Methods (continued).

Table S1 Oligonucleotides used in this study.

Table S2 Results of differential gene expression analysis for Col-0 (Col), *TPR1* Col, *TPR1 eds1*, and *TPR1 sid2*.

Table S3 Placement of genes differentially expressed between Col, *TPR1* Col, *TPR1 eds1*, and *TPR1 sid2* in different clusters after hierarchical clustering of their expression profiles.

Table S4 Results of the Gene Ontology (GO) term enrichment analysis on gene clusters in Table S2.

Table S5 Annotation of TPR1-GFP peaks called in *TPR1* Col ChIP-Seq.

Table S6 Results of the GO term enrichment analysis on genes associated with TPR1 peaks in *TPR1* Col.

Table S7 Annotation of TPR1-GFP peaks called in *TPR1 eds1* ChIP-Seq.

Table S8 Results of the GO term enrichment analysis on genes associated with TPR1 peaks in *TPR1 eds1*.

Table S9 Differential TPR1 enrichment at the chromatin regions in *TPR1* Col and *TPR1 eds1*.

Table S10 TPR1-binding categories according to Fig. 2(e) with Gene IDs

Table S11 Overlap between DEGs in different datasets and TPR1 targets from Fig. 2(e).

Table S12 Results of the differential gene expression analysis for Col-0 (Col), Col-0 *eds1-2* (*eds1*), *tpr1*, and *tpr1 tpl tpr4* (*t3*) at 0, 8, and 24 h after infection with *Pst avrRps4*.

Table S13 Results of the gene set expression analysis for Col, *eds1*, *tpr1*, and *t3* at 0, 8, and 24 h, respectively, after infection with *Pst avrRps4*.

Please note: Wiley is not responsible for the content or functionality of any Supporting Information supplied by the authors. Any queries (other than missing material) should be directed to the *New Phytologist* Central Office.